Decoding the IGF1 Signaling Gene Regulatory Network Behind Alveologenesis from A Mouse Model of Bronchopulmonary Dysplasia

Gao F[1], Li C[1], Smith SM[1], Peinado N[1], Kohbodi G[1], Tran E[2,3], Loh E[4], Li W[5], Borok Z[6] and Minoo P[1,7]

1- *Division of Neonatology, Department of Pediatrics, LAC+USC Medical Center and Children's Hospital Los Angeles, Los Angeles, CA 90033, USA.*

2- *Norris Comprehensive Cancer Center, Keck School of Medicine, USC, Los Angeles, CA 90033, USA.*

3- *Department of Biochemistry and Molecular Medicine, Keck School of Medicine, USC, Los Angeles, CA 90033, USA.*

4- *Norris Medical Library, University of Southern California, Los Angeles, CA 90089, USA.*

5- *Department of Nephrology, Jiangsu Provincial Hospital of Traditional Chinese Medicine, Nanjing 210004, China.*

6- *Division of Pulmonary, Critical Care and Sleep Medicine, Department of Medicine, University of California, San Diego, La Jolla, CA 92093, USA.*

7- *Hastings Center for Pulmonary Research, Keck School of Medicine of University of Southern California, Los Angeles, CA, 90033, USA.*

*Authors for correspondence: fremontgao@gmail.com and minoo@usc.edu

Summary

Lung development is precisely controlled by underlying Gene Regulatory Networks (GRN). Disruption of genes in the network can interrupt normal development and cause diseases such as bronchopulmonary dysplasia (BPD)–a chronic lung disease in preterm infants with morbid and sometimes lethal consequences characterized by lung immaturity and reduced alveolarization.

Here, we generated a transgenic mouse exhibiting a moderate severity BPD phenotype by blocking IGF1 signaling in secondary crest myofibroblasts (SCMF) at the onset of alveologenesis. Using approaches mirroring the construction of the model GRN in sea urchin's development, we constructed the IGF1 signaling network underlying alveologenesis using this mouse model that phenocopies BPD. The constructed GRN, consisting of 43 genes, provides a bird's-eye view of how the genes downstream of IGF1 are regulatorily connected. The GRN also reveals a mechanistic interpretation of how the effects of IGF1 signaling are transduced within SCMF from its specification genes to its effector genes and then from SCMF to its neighboring alveolar epithelial cells with WNT5A and FGF10 signaling as the bridge. Consistently, blocking WNT5A signaling in mice phenocopies BPD as inferred by the network. A comparative study on human samples suggests that a GRN of similar components and wiring underlies human BPD.

Our network view of alveologenesis is transforming our perspective to understand and treat BPD. This new perspective calls for the construction of the full signaling GRN underlying alveologenesis, upon which targeted therapies for this neonatal chronic lung disease can be viably developed.

Introduction

Development is precisely controlled by the genetic program encoded in the genome and is governed by genetic interactions (Davidson et al., 2002; Levine and Davidson, 2005). Elucidating the network of interactions among genes that govern morphogenesis through development is one of the core challenges in contemporary functional genomics research (Przybyla and Gilbert, 2021). These networks are known as developmental gene regulatory networks (GRN) and are key to understanding the developmental processes with integrative details and mechanistic perspectives. Over the past few decades, great advances have been made in decoding these networks in classical model systems (i.e. Dequeant and Pourquie, 2008; Longabaugh et al., 2017; Olson, 2006; Satou et al., 2009; Sauka-Spengler and Bronner-Fraser, 2008), as well as in forming in-depth understandings of the general design principles of these networks in development and evolution (Carre et al., 2017; Davidson, 2010; Erwin and Davidson, 2009; Gao and Davidson, 2008; Lim et al., 2013; Peter and Davidson, 2009; Royo et al., 2011). Highlighted among them is the sea urchin developmental GRN, the most comprehensive and authenticated network constructed to date (Peter and Davidson, 2017).

Disruption of any gene in the network could interrupt normal development and conceivably cause diseases. Some diseases are caused by single gene disorders while others are complex and multifactorial such as bronchopulmonary dysplasia (BPD), a common cause of morbidity and mortality in preterm infants characterized by arrested alveolar development with varied severities within the subjects' lungs (Jain and Bancalari, 2014; Jobe, 1999; Short et al., 2007). Both prenatal insults and postnatal injury increase the risk of BPD. The multifactorial etiology of BPD has made the development of therapies a unique challenge, and currently, no effective treatment exists to prevent or cure this debilitating disease.

In recent clinical trials, therapy with recombinant human insulin-like growth factor 1 (rhIGF1) protein showed initial promise for BPD, but significant limitations did not allow further clinical trials (Ley et al., 2019; Seedorf et al., 2020). One impediment to further development of IGF1 as a therapy is the lack of comprehensive information regarding the precise role of the IGF1 signaling pathway in alveologenesis.

Alveolar development is a highly complex process that is driven by multiple signaling pathways including TGFB, SHH, WNT, PDGF, VEGF, HGF, NOTCH, BMP, and IGF1 (Juul et al., 2020; Nabhan et al., 2018; Tsao et al., 2016; Verheyden and Sun, 2020; Wu and Tang, 2021; Zepp and Morrisey, 2019). IGF1 and IGF1R expression is found throughout fetal lung development and fluctuates at different stages. Both *IGF1* and *IGF1R* expression is significantly reduced in BPD lungs (Hellstrom et al., 2016; Lofqvist et al., 2012; Yilmaz et al., 2017), suggesting a potential role in the pathogenesis of BPD. The function of IGF1 and IGF1R has been examined in their respective constitutive and conditional knockout mice, but their specific function during alveologenesis has not been examined (Epaud et al., 2012; Lopez et al., 2016; Lopez et al., 2015). A recent study found interruption in IGF1 signaling compromised mechanosignaling and interrupted alveologenesis (He et al., 2021).

In our study here, we found *Igf1* and *Igf1r* are primarily expressed in SCMF in postnatal mice lungs. As a result, we interrupted IGF1 signaling in SCMF by the inactivation of *Igf1r* at the onset of alveologenesis in postnatal day 2 (PN2) mouse neonates and analyzed the resulting phenotypes. Inactivation of *Igf1r* resulted in mutant lungs with simplified and immature alveolar structure resembling that of human BPD at a moderate severity (Short et al., 2007). We reasoned that the phenotype caused by the inactivation of *Igf1r* in SCMF reflects interruption in the genetic program downstream of IGF1 signaling that drives the normal functions of SCMF in the process of alveologenesis. Alterations in SCMF may further impact

specification/differentiation of other key cell types, particularly the alveolar epithelial cells. We aim to decode the genes and their interactions behind this underlying genetic program.

Taking advantage of the high throughput next generation sequencing, people have been trying to build GRNs by computational analysis using wild type gene expression data (i.e. Jia et al., 2017; Xu et al., 2012). Currently, the most reliable way is still to build GRN experimentally on data from perturbation analyses.

Genes we particularly focus on are the regulatory genes. These genes decide the outcome of a GRN as they regulate and control other genes' expression forming a regulatory circuitry of varied hierarchy with structural and cellular genes as their terminal targets (Davidson, 2010; Erwin and Davidson, 2009). Their functions are defined by their logical control over the circuitry's operation and their synergetic biological effects are manifested by the effector genes under the circuitry (Peter and Davidson, 2009; Peter et al., 2012).

We followed the protocol similar to that used in the construction of the sea urchin GRN (Materna and Oliveri, 2008): regulatory genes were selected at the transcriptomic scale from the LungMAP database (www.lungmap.net) where their expression during alveologenesis was reported; the cellular expression patterns of these genes were then annotated on lungMAP scRNAseq data for the screen of SCMF genes; the regulatory interactions among these genes were subsequently examined from in vivo and in vitro perturbations; and cellular communications were finally determined by Secretome-Receptome analysis. Combining this data, we constructed the IGF1 signaling gene regulatory network underlying alveologenesis from this mouse model of human BPD phenocopy.

Our GRN work on alveologenesis represents a transformative view of how to understand and perhaps even design future preventive and therapeutic strategies for BPD treatment.

Results

Postnatal Expression of *Igf1* and *Igf1r* in the lung.

To define the expression pattern of *Igf1* and *Igf1r* during early postnatal lung development, we performed RT-PCR using total lung RNA from embryonic day E18 to postnatal day PN30. The analysis showed *Igf1* is expressed dynamically during development, peaking at the onset of alveologenesis and progressively decreasing thereafter (Fig.1A). The expression pattern of *Igf1r* was biphasic, initially displaying an overlap with *Igf1* in early alveologenesis with a subsequent peak occurring on PN21 (Fig.1B). Expression profiling of Igf1 and Igf1r from the entire lung and within Myofibroblasts during lung development was calculated based on data from the LungMAP (Figure 1-Figure Supplement 1A) and from the latest scRNAseq dataset (Figure 1-Figure Supplement 1B, Negretti et al., 2021). Similar patterns of their expression were observed when compared to our data.

Alveologenesis is characterized by secondary septa/crest formation, and the Alveolar Myofibroblasts are recognized as the driving force behind it. Secondary Crest Myofibroblast was derived from this concept and is broadly adopted in independent publications (i.e. Bostrom et al., 1996; Li et al., 2015; Li et al., 2018; Sun et al., 2022; Zepp et al., 2021).

The definition, specification, and function of SCMFs have not been systematically characterized. Presently, a consensus marker for these cells hasn't been established although a list of markers, such as *Acta2* (Kugler et al., 2017), *Stc1* (Zepp et al., 2021), *Tagln* (Li et al., 2018), *Fgf18* (Hagan et al., 2020) and *Pdgfra* (Li et al., 2015) have been suggested from previous work. To help resolve this issue, we compiled a comprehensive list of these markers suggested from literature and examined their expression across different mesenchymal cell types as clustered on the two latest scRNAseq datasets (Figure 1-Figure Supplement 1C&F, Negretti et al., 2021, Zepp et al., 2021). *Pdgfra* was revealed as a good SCMF marker agreed by both datasets (Figure 1-Figure Supplement 1C&F). RNAscope showed highly overlapping localization of *Igf1*/*Igf1r* and *Pdgfra* (Fig.1C&D), indicating SCMF as a principal cellular site of *Igf1* and *Igf1r* expression in lungs undergoing alveologenesis.

Mesodermal-specific Inactivation of *Igf1* and *Igf1r*.

As SCMF are derived from the lung mesenchyme early in lung development and *Dermo1* is activated at the onset of mesodermal lineage specification (Li et al., 2008), we used *Dermo1-cre* (*Dcre*) to inactivate *Igf1* and *Igf1r* separately, specifically within mesodermal lineages, and examined the mutant lung phenotype during embryonic and postnatal development (Figure 2-Figure Supplement 1A).

Loss of *Igf1* or *Igf1r* in mesodermal progenitors using floxed alleles of these genes decreased their mRNA by approximately two folds (Figure 2-Figure Supplement 1B). Consistent with previous reports (Epaud et al., 2012; Lopez et al., 2015), reduction in body weight was observed in our *Igf1r* mutant pups (Figure 2-Figure Supplement 1C&D).

The *Dcre;Igf1r-f/f* mutant displayed clearly visible lung defects: thickened saccular walls at E18; dilated sacculi and severe reductions in the number of secondary crests at PN14 with the latter extending into PN30 (Figure 2-Figure Supplement 1E). Similar defects of less severity were observed in the *Dcre;Igf1-f/f* mutant (Figure 2-Figure Supplement 1F). However, due to the timing of *Dermo1-cre* activation, it is difficult to determine whether the impact of *Igf1r* on alveologenesis occurs postnatally or is a carryover impact of events occurring prior to onset of alveologenesis.

Postnatal inactivation of *Igf1r* in SCMF profoundly arrests alveologenesis.

The SHH targeted (i.e. Gli1+) fibroblasts have been rigorously examined through lineage tracing using *Gli1creERT2;mTmG* in our lab (i.e. Li et al., 2015, Li et al., 2019). Cell lineage analysis shows the SHH signaling targets different mesenchymal cell lineages through lung development.

There was a window of time in the early postnatal stage during which the derived GFP+ cells were observed primarily localized to the secondary septa and secondarily to parabronchial & perivascular smooth muscle fibers (Li et al., 2015). When Tamoxifen was titrated down to a certain dosage, the smooth muscle fibers were no longer labeled by GFP (Figure 2-Figure Supplement 2C). This very specific regimen was employed in our current paper. Consistent with our observation, it was found that Gli1 is predominantly expressed by proliferative SCMF/Myofibroblast cells as calculated from the two largest scRNAseq datasets recently published (Figure 1-Figure Supplement 1D&G; Negretti et al., 2021; Zepp et al., 2021).

Using *Gli1-creERT2 (Gcre)*, we inactivated floxed alleles of *Igf1r* on PN2 at the onset of alveologenesis (Fig.2A). Inactivation of *Igf1r* was validated by genotyping (Figure 2-Figure Supplement 2A) and its downregulation verified by RT-PCR with RNA from both entire lung and FACS-isolated SCMF (Figure 2-Figure Supplement 2B). A successful recombination was assessed by Cre-induced green fluorescent protein (GFP) (Figure 2-Figure Supplement 2C). The mutant mice were slightly runted compared to the controls (Figure 2-Figure Supplement 2D).

Histology of multiple *Gcre;Igf1r-f/f* lungs at the timepoints PN7, PN14, and PN30, revealed a phenotype of profoundly arrested alveolar formation as measured by the mean linear intercept (MLI) (Fig.2B). In addition, ImageJ analysis showed decreased perimeter to area ratio of airspace (Peri/Area) as well as the number of airspaces per unit of area (# of Airspace/Area) – all consistent with the alveolar hypoplasia phenotype in the mutant lungs (Fig.2B, Figure 2-Figure Supplement 2E,F). The largest deviation between the controls and mutants in these measurements occurred at PN14, which marks the midpoint in the alveologenesis phase. Still, the severity of hypoplasia here is eclipsed by that seen in *Gcre;Tgfbr-f/f* induced BPD phenocopies (Gao et al., 2022).

Immunohistochemical analysis revealed no significant gross changes between the control and mutant lungs in either proliferation or apoptosis (Figure 2-Figure Supplement 2G). Similarly, examination of specific markers for various lung alveolar cell lineages, including the mesenchyme (ELN, TPM1), myofibroblasts (ACTA2, PDGFRA), endothelial cells (EMCN), lipofibroblasts (ADRP), epithelial cells (NKX2.1, SFTPC, HOPX), and pericytes (NG2) did not reveal significant differences (Fig.2C, Figure 2-Figure Supplement 2H). Nonetheless, it was observed in the mutant lungs that the deposition of elastin seemed aggregated at the secondary crest tips and the number of AT1 and AT2 cells were reduced (Fig.2C). The altered elastin deposition has been reported in previous studies (He et al., 2021; Li et al., 2019), but whether this alteration is the cause or the consequence of the impaired alveolar formation remains unknown.

To examine the genetic changes in *Gcre;Igf1r-f/f* mutant lungs, we tested two selected groups of genes: lung signature (Figure 2-Figure Supplement 2I) and angiogenesis (Figure 2-Figure Supplement 2J) genes. The analysis showed significant alterations in a few genes including *Fgf10*, *Igf1r*, and *Pdgfra* in the mutant lungs. It is noteworthy that the RNA used in the test was from whole lung tissue, while inactivation of *Igf1r* by *Gcre* was only targeted to SCMF. To determine the cell specific impacts of *Igf1r* inactivation, we characterized gene expression in FACS sorted cells in the following studies.

Identification of SCMF genes altered in mouse lungs of BPD phenotype.

Both GFP+ (SCMF) and Tomato+ (non-SCMF) cells were isolated by FACS from lungs dissected from *Gcre;mTmG* (control) and *Gcre;mTmG;Igf1r-f/f* (mutant) mice. Using the sorted cells, we compared the gene expression between them to identify genes enriched within SCMFs, those altered within SCMFs, and those altered within non-SCMFs in the mutant lungs (Fig.3A, Figure 3-Figure Supplement 1A).

Our analysis didn't focus on the components of the pathway itself which are self-conserved and usually tissue-independent (Pires-daSilva and Sommer, 2003), but was instead directed at identifying genes downstream of the pathway, especially the regulatory genes through which the developmental GRN is specified (Erwin and Davidson, 2009). 47 genes known to encode signaling molecules and transcription factors were screened from the LungMAP transcriptomic database (www.lungmap.net) where they were indicated to be expressed from SCMF between PN3 to PN14 in the mouse developmental window (Figure 3-Source Data 1). Expression of the selected genes, together with 15 known SCMF cell markers and 3 non-SCMF genes (negative control), were examined and compared by quantitative RT-PCR using RNA from the sorted cells.

Three criteria were applied to identify IGF1 signaling targets within SCMF: (1) Functionally active in SCMF with its deltaCT <= 9 (relative to *Gapdh* in Ctrl_GFP, Figure 3-Source Data 1), equivalent to >= 10 copies of transcripts per cell (copies of *Gapdh* transcripts per cell based on Barber et al., 2005); (2) highly enriched in SCMF with FC >= 10, p<=0.05 (Ctrl_GFP vs Ctrl_Tomato, Fig.3B left column, Figure 3-Source Data 1); (3) significantly altered with FC >=2, p<=0.05 (Mut_GFP vs Ctrl_GFP, Fig.3B right column, Figure 3-Source Data 1).

Nineteen genes were identified that met all 3 criteria (genes highlighted red in the first column of Figure 3-Source Data 1). Spatial localization of a select number of these genes – including *Foxd1, Sox8, Tbx2, Bmper, Actc1, Wnt5a,* and *Fgf10* – in SCMF was validated by IHC (Fig.3C, Figure 3-Figure Supplement 1B) or RNAscope (Fig.3D). Consistently, *Wnt5a* was recently reported as a signature gene of SCMF (Negretti et al., 2021), and data analysis on the two latest scRNAseq datasets revealed *Wnt5a* is dominantly expressed from SCMF/Myofibroblast along with smooth muscle cells (Figure 1-Figure Supplement 1E&H).

Regulation of the latter 19 genes by Igf1 signaling was illustrated on Biotapestry (Longabaugh, 2012) as displayed in Fig.3E. Notedly, all connections were drawn directly from the signaling, whereas the regulation may happen indirectly through the cross regulation among these genes (to be examined below).

The constructed link map points to IGF1 signaling as a positive regulator for 17 out of the 19 putative downstream genes (Fig.3E). Based on their molecular and cellular functions, the 19 genes can be stratified into two separate groups. One group is comprised of regulatory genes encoding transcription factors (*Gli1, Foxd1, Tbx2, Sox8, Dermo1, Rxra*) and signaling molecules (*Fgf10, Wnt5a, Bmper, Cyr61, Pdgfra*). The second group is comprised of *Acta2, Actc1, BGN, Des, Eln, Cnn1, FN1,* and *TNC*, representing genes that encode structural & cellular molecules. Based on the GRN's hierarchical design (Erwin and Davidson, 2009), it is most likely that IGF1 signaling first targets the regulatory genes, referred to as SCMF specifiers, whose expression subsequently targets the downstream structural and cellular genes in SCMF (SCMF effectors).

Cross regulation of altered SCMF genes in the mouse BPD phenocopy model.

Within the inventory of altered SCMF genes, as defined above, are transcription factor *Foxd1,* one of the most reduced regulatory genes from our RT-PCR measurements, and two growth

factor signaling molecules, *Fgf10* and *Wnt5a*, both known to function in postnatal lung development (Chao et al., 2016; Li et al., 2020; Zhang et al., 2020). Secretome-Receptome computation using the Fantom algorithm (Ramilowski et al., 2015) revealed the cognate receptors, FGFR1/3/4 and ROR1/2, involve in FGF10 and WNT5a signaling transduction within SCMF (Fig.4B). The results were validated on bulk RNAseq (Figure 4-Figure Supplement 1A) and the latest scRNAseq datasets (Figure 4-Figure Supplement 1B,C; Figure 4-Source Data 1). WNT5A is a highly evolutionary conserved non-canonical Wnt ligand. In spite of being identified as a non-canonical ligand, it can, under certain circumstances, signal through canonical Wnt signaling pathways directly or indirectly (i.e. Mikels and Nusse, 2006). Current analysis is focused on the signaling's non-canonical aspect and does not exclude other possibilities.

To investigate the possibility of cross regulation of these genes on the other altered SCMF genes, GFP^{+} SCMFs were isolated by FACS from postnatal *Gcre;mTmG* lungs and cultured in vitro (Fig.4 A). Cultures were treated with inhibitors which target the gene or pathway of interest. The inhibitor's dose was determined from the literature and a series of testing (Figure 4-Source Data 2), and inhibition was validated by examining its target genes (Figure 4-Figure Supplement 2A). Blocking IGF1 signaling using the IGF1R inhibitor (PPP at 4uM as in Chen et al., 2017; Jin et al., 2018; Wang et al., 2019), led to altered expression of all genes – except *Gli1* – in the same direction as observed in vivo (Figure 4-Figure Supplement 2B), indicating that isolated cells in vitro recapitulate the observed in vivo findings. Expression level of Gli1 was too low to be reliably detected in culture, likely due to absence of HH signaling which in vivo is provided exclusively by the lung epithelium.

The signaling of FGF10 and the expression of *Wnt5a* and *Foxd1* were blocked in culture with the FGFR inhibitor (Infigratinib at 1uM as in Manchado et al., 2016; Nakamura et al., 2015; Wong et al., 2018), *siWnt5a* (at 20nM as in Nemoto et al., 2012; Sakisaka et al., 2015; Zhao et al., 2017) and *siFoxd1*(at 20nM as in Li et al., 2021; Nakayama et al., 2015; Wu et al., 2018) respectively, and their effects on other SCMF genes were quantified by RT-PCR (Fig.4C). Identified genes with significant change are designated as targets of the gene/pathway perturbed, and their connections are plotted on the network (Fig.4D).

The network constructed on the new perturbation data has built connections between *Wnt5a* and certain fibroblast effector genes (i.e. *Acta2, Eln*) confirming its regulatory control on fibroblast growth and development. This finding in regard to this aspect of Wnt5a's function resonates well with the clinical data from the study of some IPF patients (Martin-Medina et al., 2018). The architecture of the new construct reveals the identity of 3 transcription factors FOXD1, TBX2, and SOX8 forming a presumed connection hub. They are targeted by all 3 signaling pathways within the network and with each other as demonstrated by FOXD1's regulation of *Tbx2* and *Sox8*, likely representing a core network subcircuit (Peter and Davidson, 2009) tasked to lockdown a regulatory state so that the signaling effect from the upstream can be stabilized.

Alveolar epithelial genes are affected through WNT5a and FGF10 signaling.

As mentioned above, both AT1 and AT2 cells were reduced in *Gcre*;*Igf1r-f/f* mutant lungs (Fig.2C). To identify any genetic alterations within these cells, we analyzed our FACS-sorted Tomato+ cells (Fig.3A), in which the lung epithelial cells reside, for the expression of a broad list of known AT1/AT2 signature genes, including their canonical markers and the ones identified by

scRNAseq (i.e. Treutlein et al., 2014; Nabhan et al., 2018; LungMAP). The comparison between the control and the mutant data identified the genes as significantly altered (Fig.5A).

Since our *Gcre;Igf1r-f/f* mutant was a SCMF targeted deletion, these changes must be a secondary consequence of intercellular cross communication. Within the altered SCMF gene list there are a total of 3 ligands: *Wnt5a*, *Fgf10*, and *Cyr61* (Fig.4D). CYR61 is more commonly recognized as a matricellular protein (i.e. Lau, 2011) rather than a classical growth factor such as FGF10 and WNT5A. Secretome-Receptome analysis indicates that FGF10 and WNT5a from SCMF communicate with alveolar epithelial cells through their cognate receptors, FGFR2 and ROR1 (Fig.4B, Figure 4-Figure Supplement 1).

The intercellular connections discovered above, plus the affected epithelial genes, were also added to the network as shown in Fig.5B. Multiple evidence has shown that IGF1 signaling can promote lung epithelial growth and development (Ghosh et al., 2013; Narasaraju et al., 2006; Wang et al., 2018b). Our work here reveals a nearly comprehensive look at the genetic pathway behind that.

WNT5a is required for alveolar formation as inferred by the IGF1 signaling GRN.

Our effort so far has led to construction of the IGF1 signaling GRN during alveologenesis. The network offers firstly a bird's-eye view of how the genes involved in IGF1 signaling are connected in the form of a molecular circuitry for alveologenesis, and then a mechanistic perception of how this circuitry is initially turned on in SCMF for the function of these cells and then advances to the neighboring alveolar epithelial cells to influence their cellular activities.

Under this mechanistic view, the position where a gene is located on the architecture of the network and the connections it has with other genes manifests its role and impact on the network's operation and outcome, hence its specific biological function in the process of alveolar formation. The network makes it possible to assess and predict a gene's function before it is tested in vivo.

Mainly derived from our in vitro data, it was discovered WNT5a signaling on the current network is located immediately downstream of IGF1 and the signaling has connections with many IGF1 downstream genes (Fig.5B). This indicates WNT5A's feed-forward role on the transduction of IGF1 signaling and its biological effects. Indeed, when *Wnt5a* was inactivated postnatally in mice, the mutant lungs exhibited a BPD-like phenotype with arrested alveologenesis, similar to what was seen in the *Igf1r* mutant (Figure 5-Figure Supplement 1; Li *et al.*, 2020). Inversely, the in vivo perturbation data collected from this *Wnt5a* mutant mouse model can be used to further define the regulatory connections where WNT5A is involved on the current IGF1 GRN.

A GRN of similar components and wiring underlies human BPD.

The expression of the mouse IGF1 signaling GRN regulatory genes in SCMF was also examined in lung samples from postmortem human BPD samples (Figure 6-Source Data 1). The regulatory genes, on the upper hierarchy of the network, determine the network's outcome. In comparison to non-BPD lungs, 9 of the 12 genes examined were altered and 8 were altered in the same direction as they were defined in the mouse GRN (Fig.6). These findings indicate a genetic program of similar components and wiring underlying in human BPD.

Discussion

With massive gene expression data available (e.g., the LungMAP database) in this postgenomic era, one pressing task is to identify the function of genes, in particular, how they interact with one another (Przybyla and Gilbert, 2021). With gene regulatory network analysis as our targeted approach, we have constructed the IGF1 signaling GRN underlying alveologenesis using a mouse model of BPD.

The application of the GRN approach in the lung field is novel as it hasn't been previously reported. Although not all the genes on the network have been examined by perturbation and the links haven't been determined as direct or indirect, the regulatory connections running along the constructed GRN are already able to provide potential mechanistic explanation as to how the effect of IGF1 signaling is transduced from one gene to a constellation of its downstream genes, and from one cell type to another. Indeed, blocking WNT5A signaling is confirmed to produce a mouse BPD-like phenotype that mimics Igf1r-/- lungs as inferred by the network (Figure 5-Figure Supplement 1; Li *et al.*, 2020). Signaling by IGF1, FGF10 and WNT5A have long been recognized in having roles in alveologenesis (i.e. Chao et al., 2016; He et al., 2021; Li et al., 2020; Zhang et al., 2020). The present GRN reveals a full genetic program and the cross-talk among them. The fact that all these signaling pathways have connections on the specification and effector genes of both alveolar mesenchymal and epithelial cells provides a direct causal link between the signaling and alveolar development.

Behind the overall process of alveologenesis is a much larger signaling gene regulatory network where several different cell types are involved. Within the mesenchymal cell type only, it is known that blocking IGF1, WNT5a, PDGFa, and TGFb signaling leads to impairment in development of alveoli, though with varying severities (Gao et al., 2022; He et al., 2021; Li et al., 2020; Li et al., 2019; Zhang et al., 2020). The sum of these leads to the construction of the hierarchical regulatory connections of these pathways within SCMF (Fig.7). Once signaling pathways from alveolar epithelium, endothelium, and immune cells are included, a much larger and more comprehensive signaling GRN behind alveologenesis is expected to emerge.

Clinically, BPD is caused predominantly by extrinsic factors which in the first place would interfere with normal cell's extracellular activities including cell signaling and communication. From the GRN perspective, BPD is a developmental disease when the signaling GRN for alveologenesis is derailed and disrupted by these extrinsic factors (Fig.7).

The type and effect of these extrinsic factors must be taken into consideration when studying this disease. There was a reported increase in Wnt5A expression by mesenchymal cells from hyperoxia BPD models (Sucre et al., 2020)—a finding seemingly contradictory to our data on Wnt5a. The etiology of BPD is multifactorial in that it involves a plethora of factors such as lung immaturity, injury, inflammation, and genetic defects. In the injury model, the two opposite conditions, hyperoxia and hypoxia, can both cause lung injury and lead to BPD-like phenotypes. In our model, the genetic defect from the targeted genetic manipulation is the culprit behind the lungs of the BPD phenotype. It is expected that genes on the network may respond differently to these different conditions and challenges. The derailed gene expression on the network, either increased or decreased, can both disrupt the signaling GRN for alveologenesis and cause BPD.

The aforementioned network disruption may occur within different cell types, onto different signaling pathways, and upon different hierarchy of the network (Fig.7). From the network's structural view, the disruption at the higher hierarchy has greater manifestation, thus leading to a higher severity of disease. TGFB signaling, atop the whole hierarchy of the signaling GRN on

Fig.7, exhibits in its mutant mouse model the most severe BPD-like phenotype when compared to mutants from the other signaling pathways under it (Chao et al., 2017; Gao et al., 2022; He et al., 2021; Li et al., 2020; Li et al., 2019). Also, different signaling sitting at various hierarchical levels has different coverage (sum of genes under the signaling's control) on the network. If disruption occurred beyond a signaling's coverage, the treatment by targeting this signaling would be off target. IGF1 signaling is found to be in the middle hierarchical level of the constructed network (Fig.7). By targeting simply one such signaling and hoping to treat BPD altogether will surely not always work.

Our GRN view on alveologenesis presents a transformative viewing of BPD and could potentially help in designing novel strategies to prevent and treat it. As for prevention, the GRN suggests a study centered on the network's periphery with its focus on cutting off the extrinsic factors and blocking their connections to the intrinsic alveologenesis GRN. For treatment, it is a study on the network itself focusing on recovering and rescuing the signaling pathways that have been disrupted. However, all this relies on the foundational construction of the whole alveologenesis GRN—which includes all major signaling pathways involved within and between each cell type and the network assembly of the hierarchical regulatory connections among them. Though the network construction is currently not experimentally accessible in human models, our work shows the alveologenesis GRN is well conserved between mouse and human lungs. With the mouse model, the whole signaling GRN behind alveologenesis can be decoded as we did in this paper. The impact of extrinsic factors/signaling pathways and their manipulation on the network can be modeled and tested as well. The insights collected can then be used to guide health delivery for BPD clinically. The general process would then be as follows: clinical patient exams and tests are used to determine the extrinsic factors; cell type gene expression data from bronchoalveolar lavage and/or biopsy are used to reveal genes altered within the alveolar compartments in patient lungs; implied extrinsic factors and altered genes are mapped onto the alveologenesis GRN where points of network disruptions can thus be defined; therapies proven successful from mouse modeling data can then be clinically pursued to recover/rescue the disruption points in the patient.

The GRN is traditionally a network built solely on chemical interactions (RNA, DNA, protein and other chemicals). Having said that however, it has been recognized that these interactions can also happen at mechanical and electrical level (i.e. Azeloglu and Iyengar, 2015). Mechanosignaling is of particular interest in the lung as the organ itself is born to function through its non-stopping mechanical movement. New technologies, including whole genome CRISPR perturbation and screening, epigenomic profiling, high resolution ChIP-seq, spatial genomics and cis-regulatory analysis, are sprouting with their potential use for a high throughput GRN construction (i.e. Cusanovich et al., 2018; Eng et al., 2019; Sanson et al., 2018; Skene and Henikoff, 2015). Our journey to decode the alveologenesis GRN is also an adventure to construct the new generation GRNs with rising technologies.

A web resource of the network and the data presented in this paper is made available to the public: https://sites.google.com/view/the-alveologenesis-grn/home, which we hope can be used as an online repository to promote any further studies and collaborations in this direction.

424 **MATERIALS AND METHODS**

425

426 **KEY RESOURCES TABLE**

Reagent or Resource	Source	Identifier	Working Concentration
Antibodies			
ACTA2	Abcam	Cat#: AB5694	1:300
ACTC1	Santa Cruz	Cat#: SC-58670	1:100
ADRP	Abcam	Cat#: AB108323	1:200
AQP5	Alomone	Cat#: AQP-005	1:100
BMPER	Santa Cruz	Cat#: SC-377502	1:200
CAS3	Cell Signaling	Cat#: 9664	1:100
ELN	Abcam	Cat#: AB21600	1:200
EMCN	R&D Systems	Cat#: AF4666	1:100
GFP	Santa Cruz	Cat#: SC-9996	1:100
HOPX	Santa Cruz	Cat#: SC-30216	1:50
KI67	R&D Systems	Cat#: AF7649	1:50
NKX2.1	Seven Hills	Cat#: 8G7G3-1	1:50
NG2	Abcam	Cat#: AB5320	1:100
PDGFRa	Cell Signaling	Cat#: 3174	1:50
PDPN	Thermo Fisher	Cat#: 14-5381-82	1:300
RFP	Rockland	Cat#: 600-401-379S	1:300
SFTPC	Abcam	Cat#: AB3786	1:200
SOX8	Santa Cruz	Cat#: SC-374446	1:50
TBX2	Santa Cruz	Cat#: SC-514291	1:50
TPM1	Sigma Aldrich	Cat#: T2780	1:500
Chemicals and Inhibitors			
Tamoxifen	Sigma	Cat#: T5648	8mg/ml
Infigratinib	Selleckchem	Cat#: S2788	1uM
PPP	Selleckchem	Cat#: S7668	4uM

siFoxd1	Dharmacon	Cat#: L-046204-00-0005	20nM
siWnt5a	Dharmacon	Cat#: L-065584-01-0005	20nM
siRNA non-targeting	Dharmacon	Cat#: D-001810-01-05	20nM
Sequencing			
Next Ultra DNA Library Prep Kit	New England Biolabs	Cat#: E7370	
Bulk RNAseq	Millard and Muriel Jacobs Genetics and Genomics Laboratory at Caltech	GEO: GSE182886	
Mouse			
Gli1-cre^{ERT2}	The Jackson Laboratory	Cat#: 007913	
Rosa26^{mTmG}	The Jackson Laboratory	Cat#: 007676	
CAG^{Tomato}	The Jackson Laboratory	Cat#: 007914	
Dermo1-cre	The Jackson Laboratory	Cat#: 028701	
Igf1$^{(flox/flox)}$	The Jackson Laboratory	Cat#: 016831	
Igf1r$^{(flox/flox)}$	The Jackson Laboratory	Cat#: 012251	
CAG-cre^{ER}	The Jackson Laboratory	Cat#: 004453	
Wnt5a$^{(flox/flox)}$	Kuruvilla Laboratory	N/A	
Foxd1GCE	McMahon Laboratory	N/A	
RNAScope			
RNAscope® Multiplex Fluorescent Reagent Kit V2	Advanced Cell Diagnostics	Cat#: 323100	
Igf1	Advanced Cell Diagnostics	Cat#: 443901-C1	1:750
Igf1r	Advanced Cell Diagnostics	Cat#: 417561-C3	1:500
Pdgfra	Advanced Cell Diagnostics	Cat#: 480661-C2	1:750
Fgf10	Advanced Cell Diagnostics	Cat#: 446371-C1	1:750
Wnt5a	Advanced Cell Diagnostics	Cat#: 316791-C3	1:500
RNAscope® 3-	Advanced Cell	Cat#: 320881	1:1500

plex Positive Control Probe_Mm	Diagnostics		
RNAscope® 3-plex Negative Control Probe	Advanced Cell Diagnostics	Cat#: 320871	1:1500
Software and Algorithms			
Image J	NIH	https://imagej.nih.gov/ij/	
STAR 2.5	PMCID: PMC3530905	https://github.com/alexdobin/STAR	
JMP pro 15	Statistical Discovery	https://www.jmp.com/en_us/software/predictive-analytics-software.html	
Fantom5 Cell Connectome	FANTOM5 project	https://fantom.gsc.riken.jp/5/suppl/Ramilowski_et_al_2015/vis/#/hive	
Imaris	BitPlane	http://www.bitplane.com/imaris/imaris	
R 3.2	R Project	https://www.r-project.org/	
LAS X	Leica	https://www.leica-microsystems.com/products/microscope-software/p/leica-las-x-ls/	
BioTapestry	Institute for Systems Biology	http://www.biotapestry.org/	

427

428

429 **1. Mouse Breeding and Genotyping**

430 All animal studies were conducted strictly according to protocols approved by the USC
431 Institutional Animal Care and Use Committee (IACUC) (Los Angeles, CA, USA). The mice
432 were housed and maintained in pathogen-free conditions at constant room temperature (20–
433 22 °C), with a 12 h light/dark cycle, and free access to water and food. *Dermo1-cre*, *Gli1-cre*^{ERT2},
434 *Rosa26*^{mTmG}, *CAG*^{tdTomato}, *Igf1*$^{(flox/flox)}$, *Igf1r*$^{(flox/flox)}$, and *CAG-cre*^{ER} mice were purchased from the
435 Jackson Laboratory. *Foxd1GCE* mice were generated by McMahon lab at USC. *SPC*^{GFP} mice
436 were generated by Wright lab at Duke University. Wnt5a$^{(flox/flox)}$ mice were provided by
437 Kuruvilla lab at Johns Hopkins University.

438 *Dermo1-cre;Igf1*$^{(flox/flox)}$ *(Dcre;Igf1-f/f)* and *Dermo1-cre;Igf1r*$^{(flox/flox)}$ *(Dcre;Igf1r-f/f)* mice were
439 generated by breeding *Dermo1-cre with Igf1*$^{(flox/flox)}$ and *Igf1r*$^{(flox/flox)}$ respectively.

440 *Gli1-cre*^{ERT2}*;Rosa26*^{mTmG} *mice* were generated by breeding *Gli1-cre*^{ERT2} and *Rosa26*^{mTmG} mice.

441 *Gli1-cre*^{ERT2}*;Igf1r*$^{(fox/flox)}$ (*Gcre*;*Igf1r-f/f*) mice were generated by breeding *Gli1-cre*^{ERT2} mice with
442 the *Igf1r*$^{(fox/flox)}$ mice.

443 *Rosa26*^{mTmG}*;Igf1r*$^{(fox/flox)}$ *(mTmG;Igf1r-f/f)* mice were generated by breeding *Rosa26*^{mTmG} mice
444 with the *Igf1r*$^{(fox/flox)}$ mice.

445 *Gli1-cre*^{ERT2}*;Rosa26*^{mTmG}*;Igf1r*$^{(fox/flox)}$ *(Gcre;mTmG;Igf1r-f/f)* mice were generated by breeding
446 *Gli1-cre*^{ERT2}*;Igf1r*$^{(fox/flox)}$ mice with the *Rosa26*^{mTmG}*;Igf1r*$^{(fox/flox)}$ mice.

447 *Foxd1GCE;CAG*^{tdTomato}*(Fcre;Tomato)* mice were generated by breeding *Foxd1GCE* mice with
448 the *CAG*^{tdTomato} mice.

449 *CAG-cre*^{ER}*;Wnt5a*$^{(fox/flox)}$ *(Ccre;Wnt5a-f/f)* mice were generated by breeding *CAG-cre*^{ER} mice
450 with the *Wnt5a*$^{(fox/flox)}$ mice.

451 Genotyping of the transgenic mice was performed by PCR with genomic DNA isolated from
452 mouse tails. The forward (F) and reverse primers (R) for transgenic mouse genotyping are listed
453 in Figure 3-Source Data 2.

454 **2. Tamoxifen Administration**

455 A single dose of Tamoxifen (8mg/mL in peanut oil) was administered by oral gavage to neonates
456 at postnatal day 2 (PN2, 100µg per pup) with a plastic feeding needle (Instech Laboratories, PA).
457 Neonatal lungs were collected between PN7 and PN30 for morphological, immunohistochemical,
458 cellular, and molecular biological analyses.

459 **3. Mouse lung tissue**

460 Mice were euthanized by CO2 inhalation at the time of tissue harvest. Chest cavity was exposed
461 and lungs cleared of blood by perfusion with cold PBS via the right ventricle. Lungs were
462 inflated with 4% formaldehyde under constant 30cm H2O pressure and allowed to fix overnight
463 at 4°C. Tissue was dehydrated through a series of ethanol washes after which they were
464 embedded in paraffin and sectioned.

465 **4. Immunohistochemistry**

466 H&E staining was performed as usual, and morphometric measurements were made using
467 ImageJ. Immunofluorescent staining was performed as previously described using paraffin-
468 embedded lung sections (Li et al., 2019). In brief, five micrometer (*µm*) tissue sections were
469 deparaffinized, rehydrated, and subjected to antigen retrieval. After blocking with normal serum,
470 the sections were probed with primary antibodies at 4° C overnight. Combinations of Alexa
471 Fluor Plus secondary antibodies (Thermo Fisher Scientific) were applied for fluorescent
472 detection of above specific primary antibodies. Nuclei were counterstained with 4′,6-diamidino-
473 2-phenylindole (DAPI). Primary antibodies used and their sources are listed in the Key
474 Resources Table below. Images were made with Leica DMi8 fluorescence microscope and
475 processed with Leica LAS X and ImageJ.

476 **5. RNAScope**

477 Samples were fixed in 10% neutral buffered formalin, dehydrated with ethanol, and embedded in
478 paraffin wax. 5*µm* Sections from paraffin blocks were processed using standard pretreatment
479 conditions per the RNAscope multiplex fluorescent reagent kit version 2 (Advanced Cell
480 Diagnostics) assay protocol. TSA-plus fluorescein, Cy3 and Cy5 fluorophores were used at
481 different dilutions optimized for each probe. RNAScope probes used are listed in the Key
482 Resources Table below. Images were made with Leica DMi8 fluorescence microscope and
483 processed with Leica LAS X and ImageJ.

484 **6. Mouse lung single-cell dissociation**

485 Single-cell suspension was prepared as described in Adam et al. (2017) with all the procedures
486 performed on ice or in cold room. Mice were euthanized and the lungs were perfused with PBS
487 as described above. The lungs were inflated with cold active protease solution (5mM CaCl2, 10
488 mg/ml Bacillus Licheniformis protease), dissected, and transferred to a petri dish where the heart,
489 thymus, and trachea were removed. The lobes were minced using a razor blade. The minced
490 tissue was then immersed in extra cold active protease solution for 10 min and triturated using a
491 1ml pipette. This Homogenate was transferred to a Miltenyi C-tube with 5ml HBSS/DNase
492 (Hank's Balanced Salt Buffer) and the Miltenyi gentleMACS lung program was run twice on
493 GentleMACs Dissociator. Subsequently, this suspension was passed through a 100um strainer,
494 pelleted at 300g for 6 minutes, suspended in 2ml RBC (Red Blood Cell) Lysis Buffer
495 (BioLegend), and incubated for 2 min. At this point, 8ml HBSS was added and centrifuged again.
496 The pellet was suspended in HBSS, then filtered through a 30um strainer. The suspension was
497 pelleted again and finally suspended in MACS separation buffer (Miltenyi Biotec) with 2% FBS
498 for Fluorescence-activated cell sorting (FACS). Cell separation and viability were examined
499 under the microscope and through Vi-CELL Cell Counter after staining with Trypan blue.

500 **7. Flow Cytometry and Cell Sorting**

501 FACS was performed on a BD FACS Aria II at stem cell Flow Cytometry Core at the Keck
502 School of Medicine of USC. The sorting was gated on viability, singlets, GFP and/or Tomato.
503 GFP+ and/or Tomato+ cells were collected as needed. For cell culture, cells were sorted in
504 DMEM containing 10% FBS. For RNA, cells of interest were collected in Trizol-LS reagent
505 (ThermoFisher).

506 **8.Bulk RNA-seq and scRNAseq data analyses**

507 Lungs dissected from Sftpc^{GFP} mouse at PN14 were dissociated into single cell suspension and
508 GFP+ cells were sorted and collected as described above. RNA was extracted using Qiagen
509 RNeasy Micro kit and then submitted to the Millard and Muriel Jacobs Genetics and Genomics
510 Laboratory at Caltech for sequencing, which was run at 50bp, single end, and 30 million reading
511 depth. The unaligned raw reads from aforementioned sequencing were processed on the
512 PartekFlow platform. In brief, read alignment, and gene annotation and quantification, were
513 based on mouse genome (mm10) and transcriptome (GENECODE genes-release 7). Tophat2 and
514 Upper Quartile algorithms were used for mapping and normalization. The RNA-seq data have
515 been deposited with GEO under the accession number GSE182886.

516 The raw scRNAseq datasets (GSE160876 and GSE165063 from Negretti et al., 2021,
517 GSE149563 from Zepp et al., 2021) were downloaded from the SRA server. The 10x Genomics'
518 Cell Ranger pipeline was used to demultiplex raw base call (BCL) files into FASTQ files,
519 perform alignment, filtering, barcode counting, and UMI counting, combine and normalize
520 counts from multiple samples, generate feature-barcode matrices, run the dimensionality
521 reduction, clustering, and gene expression analysis using parameters once they were provided in
522 the original papers. Quality control was done additionally in Partek Flow to filter out cells with
523 excess mitochondrial reads and possible doublets and remove batch effects. Loupe Browser was
524 used for data visualization and analysis including cell clustering, cell counting, cell type
525 classification, gene expression and comparative analysis.

526 **9. Neonatal lung myofibroblast culture and treatment**

527 FACS sorted GFP+ cells from PN5 neonatal lungs of *Gli1-cre*^{ERT2}*;Rosa26*^{mTmG} mice were
528 suspended in DMEM containing 10% FBS, plated in 24-well culture plates at 50,000 cells/well,
529 and incubated at 37°C with 5% CO2 on day 1 after sorting. On day 2 after sorting, the attached
530 myofibroblasts were washed with PBS and cultured in fresh medium with inhibitors or siRNAs
531 as indicated in each experiment. The ON-TARGETplus SMARTpool siRNAs from Dharmacon
532 were used, and the transfection was done using DharmaFECT™ Transfection Reagents. On day
533 4, the cells were collected for RNA analyses. The cells were authenticated for absence of
534 contaminations.

535 **10. Real-time Quantitative Polymerase Chain Reaction (real-time RT-PCR)**

536 Neonatal mouse lung cells were collected from FACS or cell culture as described above. The
537 RNA was isolated with Direct-zol™ RNA MiniPrep kit according to the manufacturer's protocol
538 (ZYMO Research). Following RNA purification, cDNA was generated using the SuperScript IV
539 First-Strand Synthesis System (ThermoFisher). Expression of selected genes was quantified by
540 Quantitative Real Time RT-PCR performed on a Light Cycler (Roche) or 7900HT fast real-time
541 PCR system (Applied Biosystems) using SYBR green reagents (ThermoFisher). The deltaCT method
542 was used to calculate relative ratios of a target gene mRNA in mutant lungs compared to
543 littermate control lungs. *Gapdh* was used as the reference gene. Primers for each gene were
544 designed on IDT website and the specificity of their amplification was verified by their melting
545 curve. Sequences of the primers are listed in Figure 3-Source Data 2.

546 **11. Human neonatal lung samples**

547 BPD and non-BPD postnatal human lung tissues were provided by the International Institute for
548 the Advancement of Medicine and the National Disease Research Interchange, and were
549 classified exempt from human subject regulations per the University of Rochester Research
550 Subjects Review Board protocol (RSRB00056775).

551 **12. Secretome-Receptome analyses**

552 Cell to cell communications were predicted using a published Fantom5 Cell Connectome dataset
553 linking ligands to their receptors (STAR Methods) (Ramilowski et al., 2015). The ligands and
554 receptors were identified from the following bulk RNAseq datasets: GSE126457 for SCMF (Li
555 et al., 2019), GSE182886 for AT2 (submitted with this paper), GSE106960 for AT1 (Wang et al.,
556 2018a), and the following scRNAseq datasets: GSE160876 (Schuler et al., 2021), GSE165063
557 (Negretti et al., 2021), and GSE149563 (Zepp et al., 2021). The IGF1 signaling GRN was drawn
558 in BioTapestry software developed by Longabaugh et al., 2012.

559 **13. Quantification and Statistical Analysis**

560 In gene expression quantification using RT-PCR, at least three biological replicates (in different
561 cases including lungs/FACS sorted cells/cultured cells) for each experimental group (Ctrl vs Mut,
562 FACS sorted cell lineage #1vs #2, treated vs untreated, BPD vs nonBPD) were used.
563 Measurement for each biological replicate was repeated three times. The Ct (cycle threshold)
564 was normalized to *Gapdh*, and the final result was presented as deltaCt or fold change. In
565 morphometric quantification and cell counting, four lungs for each experimental group (Ctrl vs
566 Mut) were used. Left lobe and right inferior lobe from each lung were targeted. Five images from
567 each lobe after staining were analyzed for morphometric quantification (at 10x magnification)
568 and cell counting (at 40x magnification). A two-tailed Student's t-test was used for the
569 comparison between two experimental groups and a one-way ANOVA was used for multiple

comparisons. Quantitative data are presented as mean values +/-SD. Data were considered significant if $p < 0.05$.

Acknowledgements: We thank Dr. Andrew P. McMahon (Keck School of Medicine of USC) for providing the *Foxd1GCE;CAG*^{tdTomato} mice. We thank Dr. Gloria S. Pryhuber (University of Rochester Medical Center) for providing the human BPD samples. We thank Arnold Sipos (Keck School of Medicine of USC) for help with imaging and Sean Gao (Arcadia High School/Duke University) for data analysis, editing, and the construction of the Alveologenesis GRN website.

Competing Interests: No.

Fundings: This work was supported by the National Institutes of Health [HL144932, HL122764 (C.L.& P.M.), HL143059 (P.M.), R35 HL135747 (Z.B.& P.M.)], the Hastings Foundation (P.M., Z.B.).

Data Availability Statement: Additional data that support the findings of this study are available on request from the corresponding author.

586 **REFERENCES**

587 Adam, M., Potter, A.S., Potter, S.S., 2017. Psychrophilic proteases dramatically reduce single-cell RNA-seq
588 artifacts: a molecular atlas of kidney development. Development 144, 3625-3632.

589 Azeloglu, E.U., Iyengar, R., 2015. Signaling networks: information flow, computation, and decision making. Cold
590 Spring Harb Perspect Biol 7, a005934.

591 Barber, R.D., Harmer, D.W., Coleman, R.A., Clark, B.J., 2005. GAPDH as a housekeeping gene: analysis of
592 GAPDH mRNA expression in a panel of 72 human tissues. Physiol Genomics 21, 389-395.

593 Bostrom, H., Willetts, K., Pekny, M., Leveen, P., Lindahl, P., Hedstrand, H., Pekna, M., Hellstrom, M., Gebre-
594 Medhin, S., Schalling, M., Nilsson, M., Kurland, S., Tornell, J., Heath, J.K., Betsholtz, C., 1996. PDGF-A signaling
595 is a critical event in lung alveolar myofibroblast development and alveogenesis. Cell 85, 863-873.

596 Carre, C., Mas, A., Krouk, G., 2017. Reverse engineering highlights potential principles of large gene regulatory
597 network design and learning. NPJ Syst Biol Appl 3, 17.

598 Chao, C.M., Moiseenko, A., Zimmer, K.P., Bellusci, S., 2016. Alveologenesis: key cellular players and fibroblast
599 growth factor 10 signaling. Mol Cell Pediatr 3, 17.

600 Chao, C.M., Yahya, F., Moiseenko, A., Tiozzo, C., Shrestha, A., Ahmadvand, N., El Agha, E., Quantius, J., Dilai,
601 S., Kheirollahi, V., Jones, M., Wilhem, J., Carraro, G., Ehrhardt, H., Zimmer, K.P., Barreto, G., Ahlbrecht, K.,
602 Morty, R.E., Herold, S., Abellar, R.G., Seeger, W., Schermuly, R., Zhang, J.S., Minoo, P., Bellusci, S., 2017. Fgf10
603 deficiency is causative for lethality in a mouse model of bronchopulmonary dysplasia. J Pathol 241, 91-103.

604 Chen, L., Chen, Q., Rong, P., Wang, H.Y., Chen, S., 2017. The energy sensing LKB1-AMPKalpha1 pathway
605 regulates IGF1 secretion and consequent activation of the IGF1R-PKB pathway in primary hepatocytes. FEBS J
606 284, 2096-2109.

607 Cusanovich, D.A., Hill, A.J., Aghamirzaie, D., Daza, R.M., Pliner, H.A., Berletch, J.B., Filippova, G.N., Huang, X.,
608 Christiansen, L., DeWitt, W.S., Lee, C., Regalado, S.G., Read, D.F., Steemers, F.J., Disteche, C.M., Trapnell, C.,
609 Shendure, J., 2018. A Single-Cell Atlas of In Vivo Mammalian Chromatin Accessibility. Cell 174, 1309-1324
610 e1318.

611 Davidson, E.H., 2010. Emerging properties of animal gene regulatory networks. Nature 468, 911-920.

612 Davidson, E.H., Rast, J.P., Oliveri, P., Ransick, A., Calestani, C., Yuh, C.H., Minokawa, T., Amore, G., Hinman,
613 V., Arenas-Mena, C., Otim, O., Brown, C.T., Livi, C.B., Lee, P.Y., Revilla, R., Rust, A.G., Pan, Z., Schilstra, M.J.,
614 Clarke, P.J., Arnone, M.I., Rowen, L., Cameron, R.A., McClay, D.R., Hood, L., Bolouri, H., 2002. A genomic
615 regulatory network for development. Science 295, 1669-1678.

616 Dequeant, M.L., Pourquie, O., 2008. Segmental patterning of the vertebrate embryonic axis. Nat Rev Genet 9, 370-
617 382.

618 Eng, C.L., Lawson, M., Zhu, Q., Dries, R., Koulena, N., Takei, Y., Yun, J., Cronin, C., Karp, C., Yuan, G.C., Cai,
619 L., 2019. Transcriptome-scale super-resolved imaging in tissues by RNA seqFISH. Nature 568, 235-239.

620 Epaud, R., Aubey, F., Xu, J., Chaker, Z., Clemessy, M., Dautin, A., Ahamed, K., Bonora, M., Hoyeau, N., Flejou,
621 J.F., Mailleux, A., Clement, A., Henrion-Caude, A., Holzenberger, M., 2012. Knockout of insulin-like growth
622 factor-1 receptor impairs distal lung morphogenesis. PloS one 7, e48071.

623 Erwin, D.H., Davidson, E.H., 2009. The evolution of hierarchical gene regulatory networks. Nat Rev Genet 10, 141-
624 148.

625 Gao, F., Davidson, E.H., 2008. Transfer of a large gene regulatory apparatus to a new developmental address in
626 echinoid evolution. Proceedings of the National Academy of Sciences of the United States of America 105, 6091-
627 6096.

628 Gao, F., Li, C., Danopoulos, S., Al Alam, D., Peinado, N., Webster, S., Borok, Z., Kohbodi, G.A., Bellusci, S.,
629 Minoo, P., 2022. Hedgehog-responsive PDGFRa(+) fibroblasts maintain a unique pool of alveolar epithelial
630 progenitor cells during alveologenesis. Cell Rep 39, 110608.

631 Ghosh, M.C., Gorantla, V., Makena, P.S., Luellen, C., Sinclair, S.E., Schwingshackl, A., Waters, C.M., 2013.
632 Insulin-like growth factor-I stimulates differentiation of ATII cells to ATI-like cells through activation of Wnt5a.
633 Am J Physiol Lung Cell Mol Physiol 305, L222-228.

634 Hagan, A.S., Zhang, B., Ornitz, D.M., 2020. Identification of a FGF18-expressing alveolar myofibroblast that is
635 developmentally cleared during alveologenesis. Development 147.

636 He, H., Snowball, J., Sun, F., Na, C.L., Whitsett, J.A., 2021. IGF1R controls mechanosignaling in myofibroblasts
637 required for pulmonary alveologenesis. JCI Insight 6.

638 Jain, D., Bancalari, E., 2014. Bronchopulmonary dysplasia: clinical perspective. Birth Defects Res A Clin Mol
639 Teratol 100, 134-144.

640 Jia, B., Xu, S., Xiao, G., Lamba, V., Liang, F., 2017. Learning gene regulatory networks from next generation
641 sequencing data. Biometrics 73, 1221-1230.

642 Jin, K., Ruan, L., Pu, J., Zhong, A., Wang, F., Tan, S., Huang, H., Mu, J., Yang, G., 2018. Metformin suppresses
643 growth and adrenocorticotrophic hormone secretion in mouse pituitary corticotroph tumor AtT20cells. Mol Cell
644 Endocrinol 478, 53-61.

645 Jobe, A.J., 1999. The new BPD: an arrest of lung development. Pediatr Res 46, 641-643.

646 Juul, N.H., Stockman, C.A., Desai, T.J., 2020. Niche Cells and Signals that Regulate Lung Alveolar Stem Cells In
647 Vivo. Cold Spring Harb Perspect Biol 12.

648 Kugler, M.C., Loomis, C.A., Zhao, Z., Cushman, J.C., Liu, L., Munger, J.S., 2017. Sonic Hedgehog Signaling
649 Regulates Myofibroblast Function during Alveolar Septum Formation in Murine Postnatal Lung. Am J Respir Cell
650 Mol Biol 57, 280-293.

651 Lau, L.F., 2011. CCN1/CYR61: the very model of a modern matricellular protein. Cell Mol Life Sci 68, 3149-3163.

652 Levine, M., Davidson, E.H., 2005. Gene regulatory networks for development. Proc Natl Acad Sci U S A 102,
653 4936-4942.

654 Ley, D., Hallberg, B., Hansen-Pupp, I., Dani, C., Ramenghi, L.A., Marlow, N., Beardsall, K., Bhatti, F., Dunger, D.,
655 Higginson, J.D., Mahaveer, A., Mezu-Ndubuisi, O.J., Reynolds, P., Giannantonio, C., van Weissenbruch, M.,
656 Barton, N., Tocoian, A., Hamdani, M., Jochim, E., Mangili, A., Chung, J.K., Turner, M.A., Smith, L.E.H.,
657 Hellstrom, A., study, t., 2019. rhIGF-1/rhIGFBP-3 in Preterm Infants: A Phase 2 Randomized Controlled Trial. J
658 Pediatr 206, 56-65 e58.

659 Li, C., Lee, M.K., Gao, F., Webster, S., Di, H., Duan, J., Yang, C.Y., Bhopal, N., Peinado, N., Pryhuber, G., Smith,
660 S.M., Borok, Z., Bellusci, S., Minoo, P., 2019. Secondary crest myofibroblast PDGFRalpha controls the
661 elastogenesis pathway via a secondary tier of signaling networks during alveologenesis. Development 146.

662 Li, C., Li, M., Li, S., Xing, Y., Yang, C.Y., Li, A., Borok, Z., De Langhe, S., Minoo, P., 2015. Progenitors of
663 secondary crest myofibroblasts are developmentally committed in early lung mesoderm. Stem Cells 33, 999-1012.

664 Li, C., Smith, S.M., Peinado, N., Gao, F., Li, W., Lee, M.K., Zhou, B., Bellusci, S., Pryhuber, G.S., Ho, H.H.,
665 Borok, Z., Minoo, P., 2020. WNT5a-ROR Signaling Is Essential for Alveologenesis. Cells 9.

666 999-1012.

667 Li, J., Yan, T., Wu, X., Ke, X., Li, X., Zhu, Y., Yang, J., Li, Z., 2021. Aberrant overexpression of transcription
668 factor Forkhead box D1 predicts poor prognosis and promotes cancer progression in HNSCC. BMC Cancer 21,
669 1205.

670 Li, M., Li, C., Liu, Y.H., Xing, Y., Hu, L., Borok, Z., Kwong, K.Y., Minoo, P., 2008. Mesodermal deletion of
671 transforming growth factor-beta receptor II disrupts lung epithelial morphogenesis: cross-talk between TGF-beta
672 and Sonic hedgehog pathways. J Biol Chem 283, 36257-36264.

673 Li, R., Bernau, K., Sandbo, N., Gu, J., Preissl, S., Sun, X., 2018. Pdgfra marks a cellular lineage with distinct
674 contributions to myofibroblasts in lung maturation and injury response. Elife 7.

675 Lim, W.A., Lee, C.M., Tang, C., 2013. Design principles of regulatory networks: searching for the molecular
676 algorithms of the cell. Mol Cell 49, 202-212.

677 Longabaugh, W.J., 2012. BioTapestry: a tool to visualize the dynamic properties of gene regulatory networks.
678 Methods Mol Biol 786, 359-394.

679 Longabaugh, W.J.R., Zeng, W., Zhang, J.A., Hosokawa, H., Jansen, C.S., Li, L., Romero-Wolf, M., Liu, P., Kueh,
680 H.Y., Mortazavi, A., Rothenberg, E.V., 2017. Bcl11b and combinatorial resolution of cell fate in the T-cell gene
681 regulatory network. Proc Natl Acad Sci U S A 114, 5800-5807.

682 Lopez, I.P., Pineiro-Hermida, S., Pais, R.S., Torrens, R., Hoeflich, A., Pichel, J.G., 2016. Involvement of Igf1r in
683 Bronchiolar Epithelial Regeneration: Role during Repair Kinetics after Selective Club Cell Ablation. PloS one 11,
684 e0166388.

685 Lopez, I.P., Rodriguez-de la Rosa, L., Pais, R.S., Pineiro-Hermida, S., Torrens, R., Contreras, J., Varela-Nieto, I.,
686 Pichel, J.G., 2015. Differential organ phenotypes after postnatal Igf1r gene conditional deletion induced by
687 tamoxifen in UBC-CreERT2; Igf1r fl/fl double transgenic mice. Transgenic Res 24, 279-294.

688 Manchado, E., Weissmueller, S., Morris, J.P.t., Chen, C.C., Wullenkord, R., Lujambio, A., de Stanchina, E., Poirier,
689 J.T., Gainor, J.F., Corcoran, R.B., Engelman, J.A., Rudin, C.M., Rosen, N., Lowe, S.W., 2016. A combinatorial
690 strategy for treating KRAS-mutant lung cancer. Nature 534, 647-651.

691 Martin-Medina, A., Lehmann, M., Burgy, O., Hermann, S., Baarsma, H.A., Wagner, D.E., De Santis, M.M., Ciolek,
692 F., Hofer, T.P., Frankenberger, M., Aichler, M., Lindner, M., Gesierich, W., Guenther, A., Walch, A., Coughlan, C.,
693 Wolters, P., Lee, J.S., Behr, J., Konigshoff, M., 2018. Increased Extracellular Vesicles Mediate WNT5A Signaling
694 in Idiopathic Pulmonary Fibrosis. Am J Respir Crit Care Med 198, 1527-1538.

695 Materna, S.C., Oliveri, P., 2008. A protocol for unraveling gene regulatory networks. Nat Protoc 3, 1876-1887.

696 Mikels, A.J., Nusse, R., 2006. Purified Wnt5a protein activates or inhibits beta-catenin-TCF signaling depending on
697 receptor context. PLoS Biol 4, e115.

698 Nabhan, A.N., Brownfield, D.G., Harbury, P.B., Krasnow, M.A., Desai, T.J., 2018. Single-cell Wnt signaling niches
699 maintain stemness of alveolar type 2 cells. Science 359, 1118-1123.

700 Nakamura, H., Arai, Y., Totoki, Y., Shirota, T., Elzawahry, A., Kato, M., Hama, N., Hosoda, F., Urushidate, T.,
701 Ohashi, S., Hiraoka, N., Ojima, H., Shimada, K., Okusaka, T., Kosuge, T., Miyagawa, S., Shibata, T., 2015.
702 Genomic spectra of biliary tract cancer. Nat Genet 47, 1003-1010.

703 Nakayama, S., Soejima, K., Yasuda, H., Yoda, S., Satomi, R., Ikemura, S., Terai, H., Sato, T., Yamaguchi, N.,
704 Hamamoto, J., Arai, D., Ishioka, K., Ohgino, K., Naoki, K., Betsuyaku, T., 2015. FOXD1 expression is associated
705 with poor prognosis in non-small cell lung cancer. Anticancer Res 35, 261-268.

706 Narasaraju, T.A., Chen, H., Weng, T., Bhaskaran, M., Jin, N., Chen, J., Chen, Z., Chinoy, M.R., Liu, L., 2006.
707 Expression profile of IGF system during lung injury and recovery in rats exposed to hyperoxia: a possible role of
708 IGF-1 in alveolar epithelial cell proliferation and differentiation. J Cell Biochem 97, 984-998.

709 Negretti, N.M., Plosa, E.J., Benjamin, J.T., Schuler, B.A., Habermann, A.C., Jetter, C.S., Gulleman, P., Bunn, C.,
710 Hackett, A.N., Ransom, M., Taylor, C.J., Nichols, D., Matlock, B.K., Guttentag, S.H., Blackwell, T.S., Banovich,
711 N.E., Kropski, J.A., Sucre, J.M.S., 2021. A single-cell atlas of mouse lung development. Development 148.

712 Nemoto, E., Ebe, Y., Kanaya, S., Tsuchiya, M., Nakamura, T., Tamura, M., Shimauchi, H., 2012. Wnt5a signaling is
713 a substantial constituent in bone morphogenetic protein-2-mediated osteoblastogenesis. Biochem Biophys Res
714 Commun 422, 627-632.

715 Olson, E.N., 2006. Gene regulatory networks in the evolution and development of the heart. Science 313, 1922-
716 1927.

717 Peter, I.S., Davidson, E.H., 2009. Modularity and design principles in the sea urchin embryo gene regulatory
718 network. FEBS Lett 583, 3948-3958.

719 Peter, I.S., Davidson, E.H., 2017. Assessing regulatory information in developmental gene regulatory networks.
720 Proc Natl Acad Sci U S A 114, 5862-5869.

721 Peter, I.S., Faure, E., Davidson, E.H., 2012. Predictive computation of genomic logic processing functions in
722 embryonic development. Proc Natl Acad Sci U S A 109, 16434-16442.

723 Pires-daSilva, A., Sommer, R.J., 2003. The evolution of signaling pathways in animal development. Nat Rev Genet
724 4, 39-49.

725 Przybyla, L., Gilbert, L.A., 2021. A new era in functional genomics screens. Nat Rev Genet.

726 Ramilowski, J.A., Goldberg, T., Harshbarger, J., Kloppmann, E., Lizio, M., Satagopam, V.P., Itoh, M., Kawaji, H.,
727 Carninci, P., Rost, B., Forrest, A.R., 2015. A draft network of ligand-receptor-mediated multicellular signaling in
728 human. Nat Commun 6, 7866.

729 Royo, J.L., Maeso, I., Irimia, M., Gao, F., Peter, I.S., Lopes, C.S., D'Aniello, S., Casares, F., Davidson, E.H.,
730 Garcia-Fernandez, J., Gomez-Skarmeta, J.L., 2011. Transphyletic conservation of developmental regulatory state in
731 animal evolution. Proceedings of the National Academy of Sciences of the United States of America 108, 14186-
732 14191.

733 Sakisaka, Y., Tsuchiya, M., Nakamura, T., Tamura, M., Shimauchi, H., Nemoto, E., 2015. Wnt5a attenuates Wnt3a-
734 induced alkaline phosphatase expression in dental follicle cells. Exp Cell Res 336, 85-93.

735 Sanson, K.R., Hanna, R.E., Hegde, M., Donovan, K.F., Strand, C., Sullender, M.E., Vaimberg, E.W., Goodale, A.,
736 Root, D.E., Piccioni, F., Doench, J.G., 2018. Optimized libraries for CRISPR-Cas9 genetic screens with multiple
737 modalities. Nat Commun 9, 5416.

738 Satou, Y., Satoh, N., Imai, K.S., 2009. Gene regulatory networks in the early ascidian embryo. Biochim Biophys
739 Acta 1789, 268-273.

740 Sauka-Spengler, T., Bronner-Fraser, M., 2008. A gene regulatory network orchestrates neural crest formation. Nat
741 Rev Mol Cell Biol 9, 557-568.

742 Schuler, B.A., Habermann, A.C., Plosa, E.J., Taylor, C.J., Jetter, C., Negretti, N.M., Kapp, M.E., Benjamin, J.T.,
743 Gulleman, P., Nichols, D.S., Braunstein, L.Z., Hackett, A., Koval, M., Guttentag, S.H., Blackwell, T.S., Webber,
744 S.A., Banovich, N.E., Vanderbilt, C.-C.C., Human Cell Atlas Biological, N., Kropski, J.A., Sucre, J.M., 2021. Age-
745 determined expression of priming protease TMPRSS2 and localization of SARS-CoV-2 in lung epithelium. J Clin
746 Invest 131.

747 Seedorf, G., Kim, C., Wallace, B., Mandell, E.W., Nowlin, T., Shepherd, D., Abman, S.H., 2020. rhIGF-1/BP3
748 Preserves Lung Growth and Prevents Pulmonary Hypertension in Experimental Bronchopulmonary Dysplasia. Am J
749 Respir Crit Care Med 201, 1120-1134.

750 Short, E.J., Kirchner, H.L., Asaad, G.R., Fulton, S.E., Lewis, B.A., Klein, N., Eisengart, S., Baley, J., Kercsmar, C.,
751 Min, M.O., Singer, L.T., 2007. Developmental sequelae in preterm infants having a diagnosis of bronchopulmonary
752 dysplasia: analysis using a severity-based classification system. Arch Pediatr Adolesc Med 161, 1082-1087.

753 Skene, P.J., Henikoff, S., 2015. A simple method for generating high-resolution maps of genome-wide protein
754 binding. Elife 4, e09225.

755 Sucre, J.M.S., Vickers, K.C., Benjamin, J.T., Plosa, E.J., Jetter, C.S., Cutrone, A., Ransom, M., Anderson, Z.,
756 Sheng, Q., Fensterheim, B.A., Ambalavanan, N., Millis, B., Lee, E., Zijlstra, A., Konigshoff, M., Blackwell, T.S.,
757 Guttentag, S.H., 2020. Hyperoxia Injury in the Developing Lung Is Mediated by Mesenchymal Expression of
758 Wnt5A. Am J Respir Crit Care Med 201, 1249-1262.

759 Sun, X., Perl, A.K., Li, R., Bell, S.M., Sajti, E., Kalinichenko, V.V., Kalin, T.V., Misra, R.S., Deshmukh, H., Clair,
760 G., Kyle, J., Crotty Alexander, L.E., Masso-Silva, J.A., Kitzmiller, J.A., Wikenheiser-Brokamp, K.A., Deutsch, G.,
761 Guo, M., Du, Y., Morley, M.P., Valdez, M.J., Yu, H.V., Jin, K., Bardes, E.E., Zepp, J.A., Neithamer, T., Basil,
762 M.C., Zacharias, W.J., Verheyden, J., Young, R., Bandyopadhyay, G., Lin, S., Ansong, C., Adkins, J., Salomonis,
763 N., Aronow, B.J., Xu, Y., Pryhuber, G., Whitsett, J., Morrisey, E.E., Consortium, N.L., 2022. A census of the lung:
764 CellCards from LungMAP. Dev Cell 57, 112-145 e112.

765 Tsao, P.N., Matsuoka, C., Wei, S.C., Sato, A., Sato, S., Hasegawa, K., Chen, H.K., Ling, T.Y., Mori, M., Cardoso,
766 W.V., Morimoto, M., 2016. Epithelial Notch signaling regulates lung alveolar morphogenesis and airway epithelial
767 integrity. Proc Natl Acad Sci U S A 113, 8242-8247.

768 Verheyden, J.M., Sun, X., 2020. A transitional stem cell state in the lung. Nat Cell Biol 22, 1025-1026.

769 Wang, G., Yin, L., Peng, Y., Gao, Y., Gao, H., Zhang, J., Lv, N., Miao, Y., Lu, Z., 2019. Insulin promotes invasion
770 and migration of KRAS(G12D) mutant HPNE cells by upregulating MMP-2 gelatinolytic activity via ERK- and
771 PI3K-dependent signalling. Cell Prolif 52, e12575.

772 Wang, Y., Tang, Z., Huang, H., Li, J., Wang, Z., Yu, Y., Zhang, C., Li, J., Dai, H., Wang, F., Cai, T., Tang, N.,
773 2018a. Pulmonary alveolar type I cell population consists of two distinct subtypes that differ in cell fate. Proc Natl
774 Acad Sci U S A 115, 2407-2412.

775 Wang, Z., Li, W., Guo, Q., Wang, Y., Ma, L., Zhang, X., 2018b. Insulin-Like Growth Factor-1 Signaling in Lung
776 Development and Inflammatory Lung Diseases. Biomed Res Int 2018, 6057589.

777 Wong, G.S., Zhou, J., Liu, J.B., Wu, Z., Xu, X., Li, T., Xu, D., Schumacher, S.E., Puschhof, J., McFarland, J., Zou,
778 C., Dulak, A., Henderson, L., Xu, P., O'Day, E., Rendak, R., Liao, W.L., Cecchi, F., Hembrough, T., Schwartz, S.,
779 Szeto, C., Rustgi, A.K., Wong, K.K., Diehl, J.A., Jensen, K., Graziano, F., Ruzzo, A., Fereshetian, S., Mertins, P.,
780 Carr, S.A., Beroukhim, R., Nakamura, K., Oki, E., Watanabe, M., Baba, H., Imamura, Y., Catenacci, D., Bass, A.J.,
781 2018. Targeting wild-type KRAS-amplified gastroesophageal cancer through combined MEK and SHP2 inhibition.
782 Nat Med 24, 968-977.

783 Wu, H., Larribere, L., Sun, Q., Novak, D., Sachindra, S., Granados, K., Umansky, V., Utikal, J., 2018. Loss of
784 neural crest-associated gene FOXD1 impairs melanoma invasion and migration via RAC1B downregulation. Int J
785 Cancer 143, 2962-2972.

786 Wu, H., Tang, N., 2021. Stem cells in pulmonary alveolar regeneration. Development 148.

787 Xu, Y., Wang, Y., Besnard, V., Ikegami, M., Wert, S.E., Heffner, C., Murray, S.A., Donahue, L.R., Whitsett, J.A.,
788 2012. Transcriptional programs controlling perinatal lung maturation. PloS one 7, e37046.

789 Zepp, J.A., Morley, M.P., Loebel, C., Kremp, M.M., Chaudhry, F.N., Basil, M.C., Leach, J.P., Liberti, D.C.,
790 Niethamer, T.K., Ying, Y., Jayachandran, S., Babu, A., Zhou, S., Frank, D.B., Burdick, J.A., Morrisey, E.E., 2021.
791 Genomic, epigenomic, and biophysical cues controlling the emergence of the lung alveolus. Science 371.

792 Zepp, J.A., Morrisey, E.E., 2019. Cellular crosstalk in the development and regeneration of the respiratory system.
793 Nat Rev Mol Cell Biol 20, 551-566.

794 Zhang, K., Yao, E., Lin, C., Chou, Y.T., Wong, J., Li, J., Wolters, P.J., Chuang, P.T., 2020. A mammalian Wnt5a-
795 Ror2-Vangl2 axis controls the cytoskeleton and confers cellular properties required for alveologenesis. Elife 9.

796 Zhao, G., Cheng, X.W., Piao, L., Hu, L., Lei, Y., Yang, G., Inoue, A., Ogasawara, S., Wu, H., Hao, C.N., Okumura,
797 K., Kuzuya, M., 2017. The Soluble VEGF Receptor sFlt-1 Contributes to Impaired Neovascularization in Aged
798 Mice. Aging Dis 8, 287-300.

799

FIGURES AND SUPPLEMENTS

Figure 1: Temporal and spatial expression of *Igf1* and *Igf1r* during neonatal lung development in mice.

A, B: Temporal expression of *Igf1* (A) and *Igf1r* (B) from E18 to PN30, quantified by RT-PCR and normalized to *Gapdh*. RNA used was collected from the whole lung and each stage was represented by at least five lungs. C: Spatial localization of mRNA for *Igf1* (C) and *Igf1r* (D) in PN7 lungs as detected by RNAscope and their overlapped expression with *Pdgfra*. Outlined area on the left is magnified on the right. Scale bars: 20um under the whole view and 10um under the magnified view.

Figure 1-Figure Supplement 1: Igf1, Igf1r and SCMF/MyoFB marker gene's expression in mouse lung from published public data sources.

A, B: Expression profiling of Igf1 and Igf1r from whole lung and in SCMF/MyoFB cells during lung development as calculated on data from LungMap (A) and from Negretti et al., 2021 (B). C-H: Heatmap and violin plots of collected SCMF/MyoFB marker gene's expression within mesenchymal sub cell clusters as calculated on data from Zepp et al., 2021 (C-E) and Negretti et al., 2021 (F-H).

Figure 2: Postnatal inactivation of *Igf1r* from lung secondary crest myofibroblast cells.

A: Schematic of the experimental protocol. B: H&E staining of lung sections from control (a-c) and *Gli1-cre*^{ERT2} mutant (d-f) mice and their morphometric measurements by MLI (g-i) and Peri/Area ratio (j-l) at PN7, PN14 and PN30. See Figure 2-Figure Supplement 1 for the definition and calculation of these indices. C: Immunostaining of lung sections from control (a-d) and mutant (e-h) mice for Elastin (a,e), ACTA2 (b,f), AQP5/HOPX (c,g) and SFTPC/PDPN (d,h), and the comparison of the number of AT1 (i) and AT2 (j) cells between the control and mutant. Scale bar: 100um in B and 25um in C. *p*-value: * stands for 0.05-0.01, ** for 0.01-0.001, *** for <0.001, n.s. for not significant.The same designation is used throughout the paper.

Figure 2-Figure Supplement 1: Mesoderm constitutive deletion of *Igf1* and *Igf1r* from mouse lung.

A: Schematic of the experimental protocol. B: Impact of inactivation of *Igf1* (left) and *Igf1r* (right) by *Dermo1-cre* on their respective transcripts in PN14 lungs. Data is represented as mean +/- SD of three lungs from each experimental group. C: Body weight variation of pups at PN14 of one single litter from the breeding of *Dermo1-cre;Igf1r-f/-* and *Igf1r-f/f* (left graph). Body weight comparison of pups between the control and the homozygous mutant (right graph). Data is represented as mean +/- SD of 4 mice from each experimental group. D: Same experiment as done in C for pups at PN30. E: H&E staining of lung sections from *Igf1r* control (a-c) and *Dermo1-cre* mutant (d-f) mice and their morphometric measurements (MLI&%Airspace – see Figure 2-Figure Supplement 2E,F for more information) (g-i) at E18, PN14, and PN30. F: H&E staining of lung sections from *Igf1* control (a-c) and *Dermo1-cre* mutant (d-f) mice and their morphometric measurements (g-i) at E18, PN14, and PN30. Scale bar: 100um for all images. *p*-value: * stands for 0.05-0.001, ** for 0.01-0.001, *** for <0.001, n.s. for not significant. The same designation is used throughout the paper.

Figure 2-Figure Supplement 2: Postnatal inactivation of *Igf1r* in secondary crest myofibroblasts.

A: genotyping of pups from the breeding between *Gli1-cre*^{ERT2};*Igf1r-f/f* and *Igf1r-f/f;mTmG* mice. B: *Igf1r* expression in control and mutant lungs at PN14 using whole lung (left) and FACS sorted GFP+ cells (right). Data is represented as mean +/- SD of three lungs from each experimental group. C: Immunostaining for Eln, Acta2, and GFP on PN14 lung sections from *Gli1-cre*^{ERT2}*;mTmG* mice which were tamoxifen-treated at PN2 with 400ug (a-c) and 100ug (d-f) per pup. Smooth muscle fibers (outlined in c&f) were labeled by GFP at higher but not at lower TAM dosage. Scale bar: 25um for all images. D: Weight comparison between Ctrl and Mut at PN14. Data is represented as mean +/- SD of three mice from each experimental group. E: A sample of how to use ImageJ on cell counting (a,b) and morphometric measurements (c,d) where number of separated airspaces (*N*), perimeter (*Peri*) and area (*Area*) of each airspace can be calculated. Scale bar: 25um in a and 100um in c. F: Morphometric comparison between Ctrl and Mut at PN14 using different indexes. MLI is defined as in Crowley et al., 2019 and the others are quantified as below: $(Peri/Area) = \sum_1^N(Peri)/\sum_1^N(Area)$, $(\#\ of\ Airspaces/Area) = N/\sum_1^N(Area)$, $\%Airspace=(Area\ of\ Airspaces/Area\ Total) = \sum_1^N(Area)/(Area\ Total)$. G: Immunostaining for Ki67 (a,b) and cleaved Caspase-3 (d,e) on control and mutant lungs at PN14. The percentage of cells identified from above staining was compared between the control and mutant (c,f). Data is represented as mean +/- SD of three lungs from each experimental group. Scale bar: 25um for all images. H: Immunostaining for mesenchymal marker ELN (a,d), TPM1 (a,d), ACTA2 (b,e), PDGFRA (h,k), epithelial marker NKX2.1 (h,k), CLDN18 (i,l), endothelial marker EMCN (b,c,e,f,g,j), lipofibroblast marker ADRP (g,j), and pericyte marker NG2 (c,f) using control and mutant lungs at PN14. Scale bar: 50um for i, l and 25um for all the other images. I: Comparative expression of selected lung marker genes between control and mutant lungs at PN14. Data is represented as mean +/- SD of three lungs from each experimental group. J: Comparative expression of angiogenesis related genes between control and mutant lungs at PN14. Data is represented as mean +/- SD of three lungs from each experimental group.

Figure 3: Identification of SCMF genes altered in *Gli1-cre*^{ERT2}*;Igf1r-f/f* mutant lungs.

A: Schematic of the experimental protocol. B: RT-PCR data from the selected genes displaying their enrichment in SCMF and alterations in the mutant. Genes marked with the orange line: regulatory genes selected from LungMap database; Genes with the green line: common SCMF markers; Genes with the blue line: non-SCMF genes. Red circles: data points meeting the cutoff criteria described in the text; Empty circles: data points failing the cutoff criteria. This designation is used throughout the manuscript. C: Spatial expression of Foxd1-Tomato/ELN (a-c), SOX8/ELN (d-f), and TBX2/ELN (g-i) in the alveolar compartment of PN14 lungs as detected by immunostaining. Specific antibodies were used for SOX8, TBX2, and ELN. RFP antibody was used for Foxd1-Tomato on lungs dissected from *Foxd1GCE;CAG*^{Tomato} mice. Scale bar: 25um for all images. D: Spatial expression of *Wnt5a/Pdgfra* (a) and *Fgf10/Pdgfra* (b) in the alveolar compartment of PN14 lungs as detected by RNAscope. Outlined area on the left is magnified on the right. Scale bars: 20um under the whole view and 10um under the magnified view. E: Biotapestry network illustration of altered SCMF genes and their connections to IGF1 signaling within SCMF. The source of IGF1 can be both autocrine and paracrine. Genes (nodes) are shown in the territories (colored boxes) in which they are expressed. Edges show regulation by the originating upstream factor and are either positive (arrow) or repressive (bar). Signalings across cell membranes are indicated as double arrow heads.

Figure 3-Figure Supplement 1: Identification of SCMF genes altered in *Gli1-cre*^{ERT2}*;Igf1r-f/f* mutant lung.

A: GFP+ and Tomato+ cells are separated by FACS. B: Spatial expression of SOX8/ELN (a-f), TBX2/ELN (g-l), BMPER/ELN (m-r), and ACTC1/ELN (s-x) in the alveolar compartment in control and mutant lungs at PN14 as detected by immunostaining. Scale bar: 25um for all images.

Figure 3-Source Data 1: Table of genes with their RT-PCR data showing their level of expression in SCMF, enrichment in SCMF, and differential expression between control and mutant lungs, and annotation of their cellular expression in the lung based on LungMAP scRNAseq data. Cells in red: data points which meet the cutoff criteria designated in the paper or the cell type where the gene is annotated as expressing.

Figure 3-Source Data 2: List of the primers used in the paper. Primers are for *Mus musculus* by default and for *Homo sapiens* when denoted with Hs.

Figure 4: Cross regulation of the altered SCMF genes.

A: Schematic of the experimental protocol. B: Flow chart of the secretome-receptome analysis among SCMF, AT1 and AT2 cells. The ligands and receptors were identified from the following RNAseq datasets: GSE126457 for SCMF (Li et al., 2019), GSE182886 for AT2, GSE106960 for AT1 (Wang et al., 2018a). C: RT-PCR data from the altered SCMF genes demonstrating their response to the treatments by Infigratinib, *siWnt5a*, and *siFoxd1*. D: Biotapestry network illustration of the cross regulation among the altered SCMF genes.

Figure 4-Figure Supplement 1: Secretome-receptome analysis of cellular communications between *IGF1*, *WNT5A* and *FGF10* ligands from SCMF and receptors from SCMF, AT2 and AT1 as calculated on different data sources: bulk RNAseq data (A), scRNAseq data from Negretti et al., 2021 (B) and scRNAseq data from Zepp et al., 2021 (C).

Receptors are rendered as magenta for those from SCMF, yellow for AT2, and cyan for AT1; are arranged based on their abundance within each cell type with higher quantities on top/left and lower quantities on bottom/right. Ligands are connected to the receptors predicted to be restrictive and decisive for the function of the respective signaling (labeled in black). Other receptors (labeled in gray) are ignored at this time due to the following: 1. their lower abundance—only the top 150 highly expressed receptors from each cell type are considered; 2. less binding affinity—i.e. IGF1R vs INSR; 3. broad expression—i.e. LRP5 and FZD proteins are ubiquitously expressed across all cell types studied here; 4. known gene spatial expression—i.e. Fgfr2 is specifically expressed in alveolar epithelium. See Figure 4-Source Data 1 for the full list of these signaling genes selected for each cell type and from each dataset.

Figure 4-Figure Supplement 2: SCMF cell culture treatments.

A: RT-PCR data showing the effect of various treatments (top) on their respective targeted genes (bottom). B: RT-PCR data from the altered SCMF genes demonstrating their response to the treatment from PPP.

Figure 4-Source Data 1: List of the ligands and receptors used for Secretome-Receptome analysis.

Figure 4-Source Data 2: List of the inhibitors and their concentrations used in cell culture treatment.

Figure 5: Epithelial genes affected in *Gli1-cre^{ERT2};Igf1r-f/f* mutant lung and their connections to IGF1 signaling from SCMF.

A: RT-PCR data from selected AT1 and AT2 genes revealing their alteration in the mutant lung. B: The IGF1 signaling GRN during alveologenesis consisting of genes downstream of IGF1 signaling from three cell types (SCMF, AT2 and AT1) and the intracellular and intercellular regulatory connections among them.

Figure 5-Figure Supplement 1: Postnatal inactivation of *Wnt5a*.

A: Schematic of the experimental protocol. B: H&E staining of lung sections obtained from control (a) and Wnt5a-/- (b) mice as generated and described in Li *et al.,* 2020 and analyzed for this study. C: Morphometric measurements by MLI (c) and Peri/Area ratio (d). Scale bar: 100um for all images.

Figure 6: Regulatory genes from IGF1 signaling GRN and their expression in human bronchopulmonary dysplasia (BPD) lungs.

Figure 6-Source Data 1: List of clinical data for human neonatal lung samples.

Figure 7: The hierarchical connections among the signaling pathways within SCMF during alveologenesis.

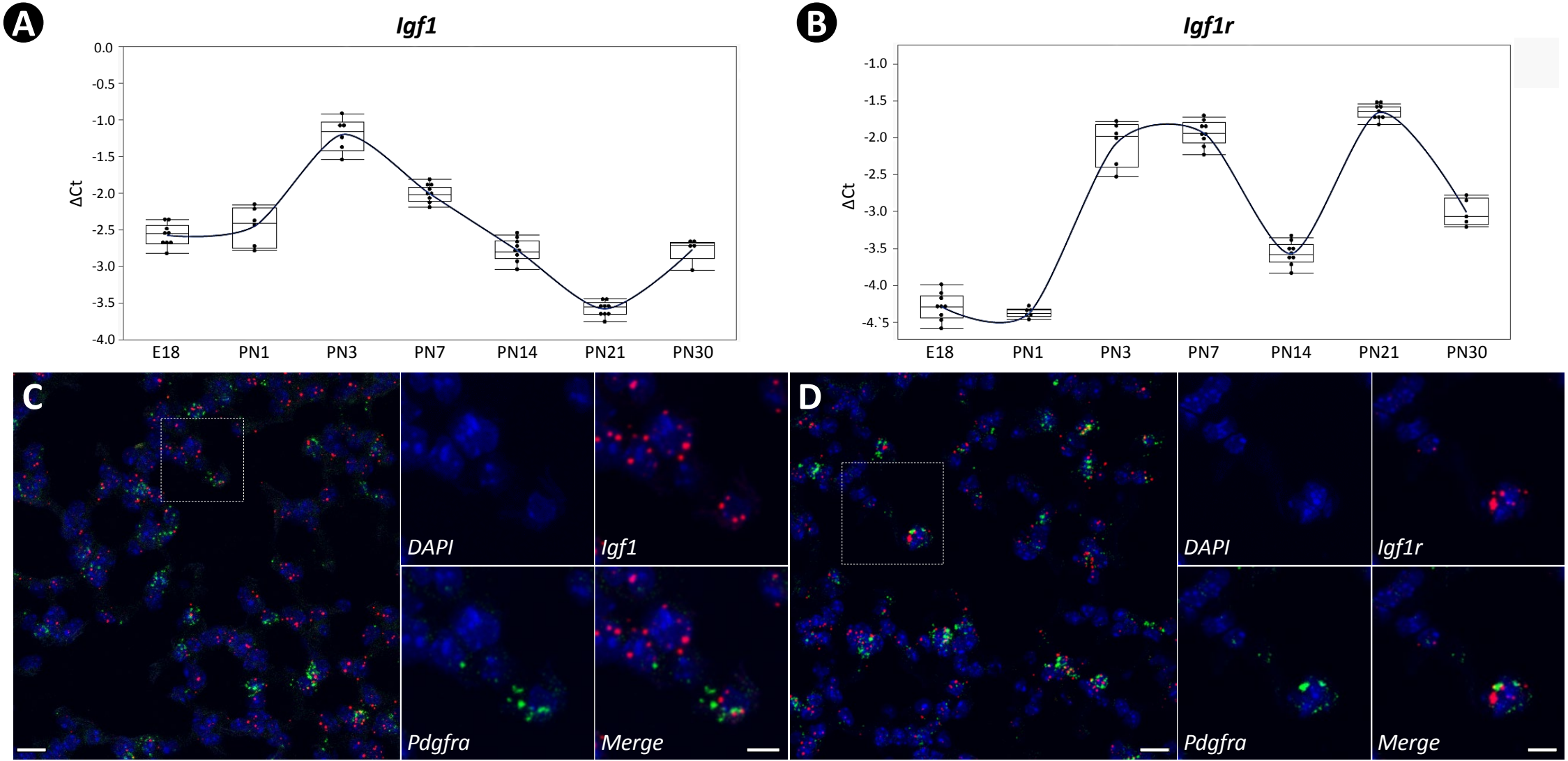
A
Igf1
ΔCt
0.0
-0.5
-1.0
-1.5
-2.0
-2.5
-3.0
-3.5
-4.0
E18
PN1
PN3
PN7
PN14
PN21
PN30
B
Igf1r
ΔCt
-1.0
-1.5
-2.0
-2.5
-3.0
-3.5
-4.0
-4.`5
E18
PN1
PN3
PN7
PN14
PN21
PN30
C
DAPI
Igf1
Pdgfra
Merge
D
DAPI
Igf1r
Pdgfra
Merge

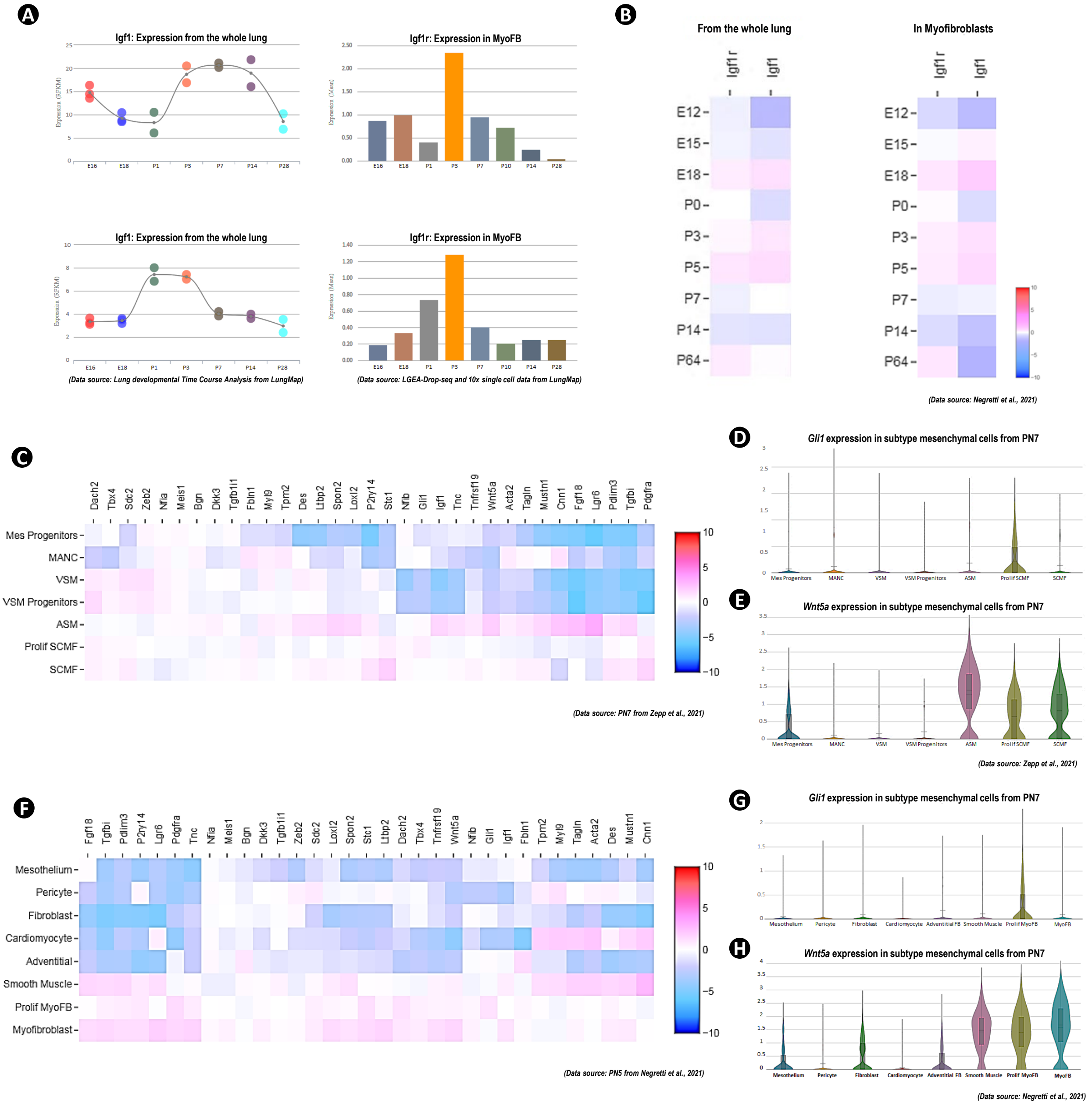
A
Igf1: Expression from the whole lung
Expression (RPKM)
E16 E18 P1 P3 P7 P14 P28
Igf1r: Expression in MyoFB
Expression (Mean)
E16 E18 P1 P3 P7 P10 P14 P28
Igf1: Expression from the whole lung
Expression (RPKM)
E16 E18 P1 P3 P7 P14 P28
Igf1r: Expression in MyoFB
Expression (Mean)
E16 E18 P1 P3 P7 P10 P14 P28
(Data source: Lung developmental Time Course Analysis from LungMap)
(Data source: LGEA-Drop-seq and 10x single cell data from LungMap)
B
From the whole lung
In Myofibroblasts
Igf1r
Igf1
E12
E15
E18
P0
P3
P5
P7
P14
P64
(Data source: Negretti et al., 2021)
C
Dach2 Tbx4 Sdc2 Zeb2 Nfia Meis1 Bgn Dkk3 Tgfb1i1 Fbln1 Myl9 Tpm2 Des Ltbp2 Spon2 Loxl2 P2ry14 Stc1 Nfib Gli1 Igf1 Tnc Tnfrsf19 Wnt5a Acta2 Tagln Mustn1 Cnn1 Fgf18 Lgr6 Pdlim3 Tgfbi Pdgfra
Mes Progenitors
MANC
VSM
VSM Progenitors
ASM
Prolif SCMF
SCMF
(Data source: PN7 from Zepp et al., 2021)
D
Gli1 expression in subtype mesenchymal cells from PN7
Mes Progenitors MANC VSM VSM Progenitors ASM Prolif SCMF SCMF
E
Wnt5a expression in subtype mesenchymal cells from PN7
Mes Progenitors MANC VSM VSM Progenitors ASM Prolif SCMF SCMF
(Data source: Zepp et al., 2021)
F
Fgf18 Tgfbi Pdlim3 P2ry14 Lgr6 Pdgfra Tnc Nfia Meis1 Bgn Dkk3 Tgfb1i1 Zeb2 Sdc2 Loxl2 Spon2 Stc1 Ltbp2 Dach2 Tbx4 Tnfrsf19 Wnt5a Nfib Gli1 Igf1 Fbln1 Tpm2 Myl9 Tagln Acta2 Des Mustn1 Cnn1
Mesothelium
Pericyte
Fibroblast
Cardiomyocyte
Adventitial
Smooth Muscle
Prolif MyoFB
Myofibroblast
(Data source: PN5 from Negretti et al., 2021)
G
Gli1 expression in subtype mesenchymal cells from PN7
Mesothelium Pericyte Fibroblast Cardiomyocyte Adventitial FB Smooth Muscle Prolif MyoFB MyoFB
H
Wnt5a expression in subtype mesenchymal cells from PN7
Mesothelium Pericyte Fibroblast Cardiomyocyte Adventitial FB Smooth Muscle Prolif MyoFB MyoFB
(Data source: Negretti et al., 2021)

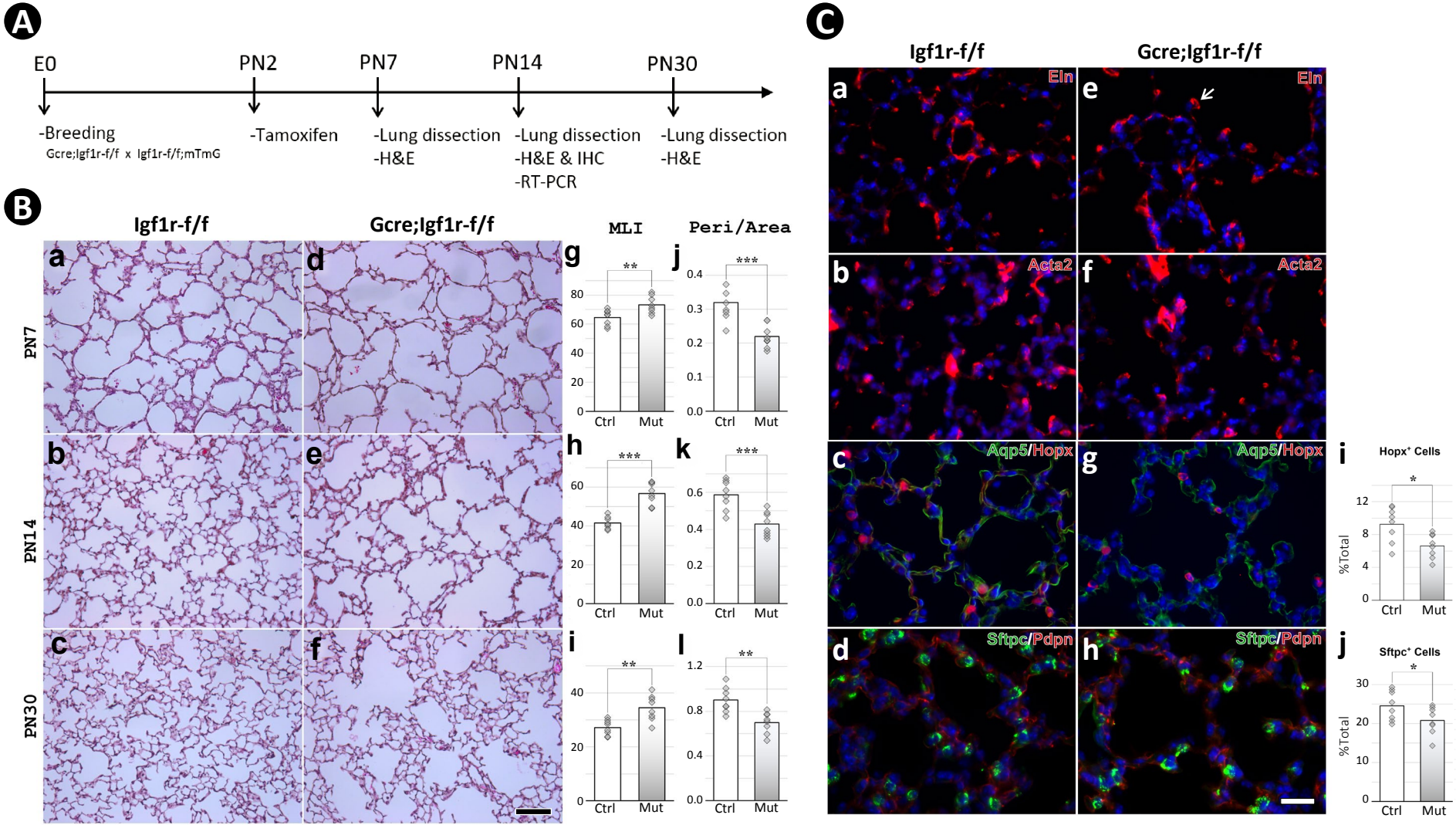
A
E0
PN2
PN7
PN14
PN30
-Breeding
Gcre;Igf1r-f/f x Igf1r-f/f;mTmG
-Tamoxifen
-Lung dissection
-H&E
-Lung dissection
-H&E & IHC
-RT-PCR
-Lung dissection
-H&E
B
Igf1r-f/f
Gcre;Igf1r-f/f
PN7
PN14
PN30
MLI
Peri/Area
Ctrl
Mut
C
Igf1r-f/f
Gcre;Igf1r-f/f
Eln
Acta2
Aqp5/Hopx
Sftpc/Pdpn
Hopx+ Cells
Sftpc+ Cells
%Total

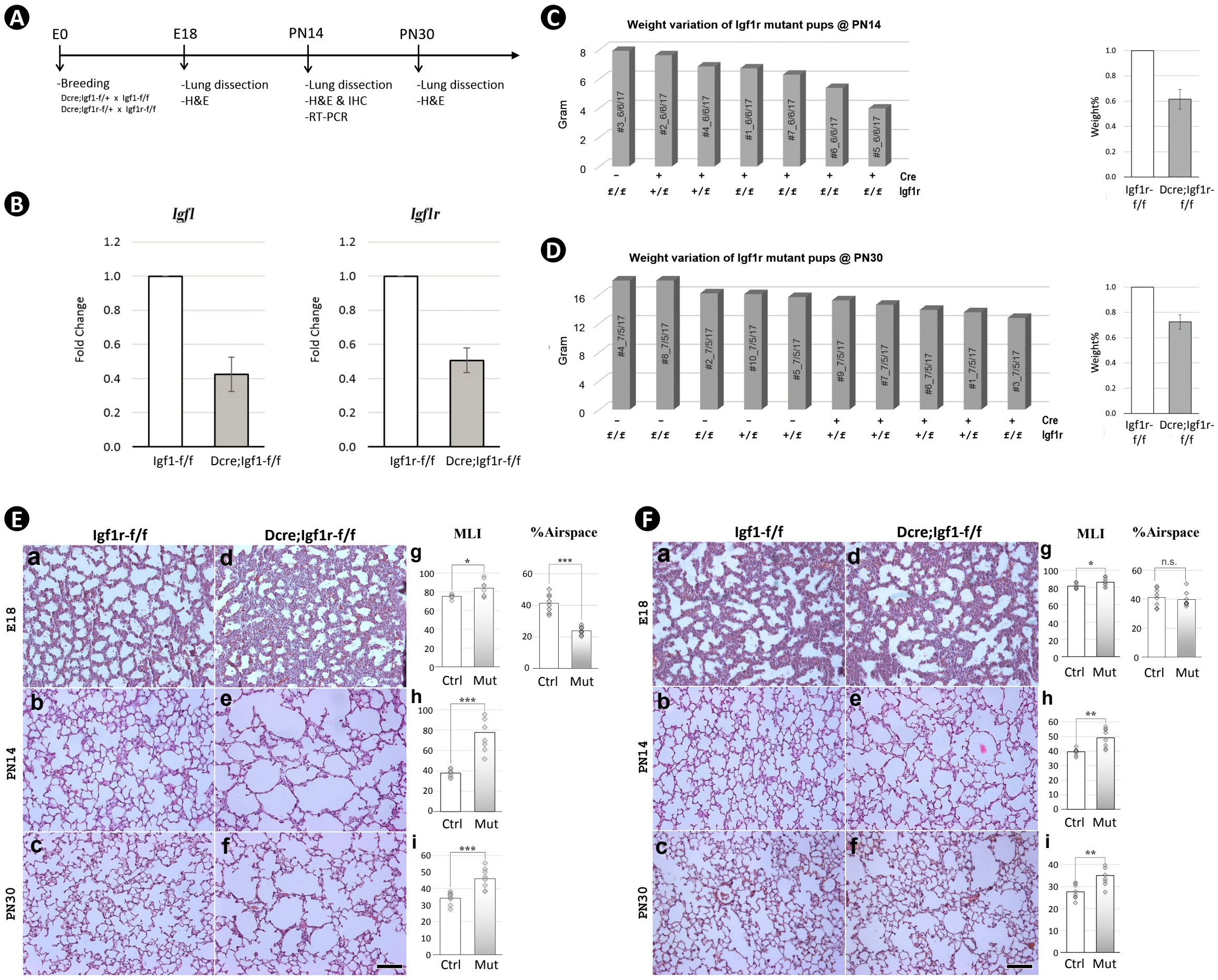
A
E0
E18
PN14
PN30
-Breeding
Dcre;Igf1-f/+ x Igf1-f/f
Dcre;Igf1r-f/+ x Igf1r-f/f
-Lung dissection
-H&E
-Lung dissection
-H&E & IHC
-RT-PCR
-Lung dissection
-H&E
B
Igf1
Igf1r
Fold Change
Igf1-f/f
Dcre;Igf1-f/f
Igf1r-f/f
Dcre;Igf1r-f/f
C
Weight variation of Igf1r mutant pups @ PN14
Gram
#3_6/6/17
#2_6/6/17
#4_6/6/17
#1_6/6/17
#7_6/6/17
#6_6/6/17
#5_6/6/17
Cre
Igf1r
Weight%
Igf1r-f/f
Dcre;Igf1r-f/f
D
Weight variation of Igf1r mutant pups @ PN30
#4_7/5/17
#8_7/5/17
#2_7/5/17
#10_7/5/17
#5_7/5/17
#9_7/5/17
#7_7/5/17
#6_7/5/17
#1_7/5/17
#3_7/5/17
E
Igf1r-f/f
Dcre;Igf1r-f/f
MLI
%Airspace
E18
PN14
PN30
Ctrl
Mut
F
Igf1-f/f
Dcre;Igf1-f/f
n.s.

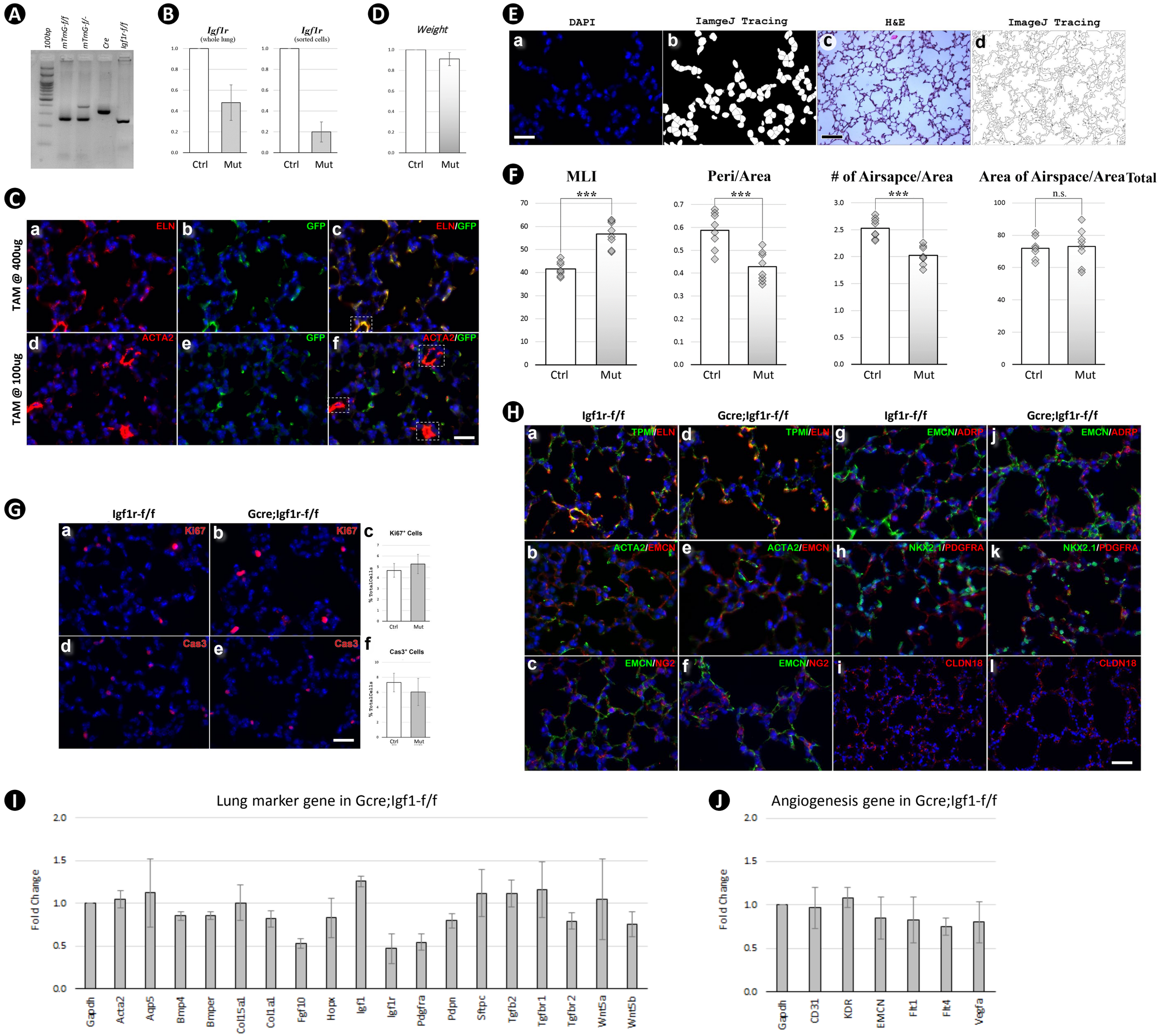
A
100bp
mTmG-f/f
mTmG-f/-
Cre
Igf1r-f/f
B
Igf1r (whole lung)
Igf1r (sorted cells)
Ctrl
Mut
D
Weight
E
DAPI
IamgeJ Tracing
H&E
ImageJ Tracing
F
MLI
Peri/Area
# of Airsapce/Area
Area of Airspace/Area Total
***
n.s.
C
TAM @ 400ug
TAM @ 100ug
ELN
GFP
ELN/GFP
ACTA2
ACTA2/GFP
G
Igf1r-f/f
Gcre;Igf1r-f/f
Ki67
Cas3
Ki67⁺ Cells
Cas3⁺ Cells
% TotalCells
H
TPM/ELN
EMCN/ADRP
ACTA2/EMCN
NKX2.1/PDGFRA
EMCN/NG2
CLDN18
I
Lung marker gene in Gcre;Igf1-f/f
Fold Change
Gapdh
Acta2
Aqp5
Bmp4
Bmper
Col15a1
Col1a1
Fgf10
Hopx
Igf1
Igf1r
Pdgfra
Pdpn
Sftpc
Tgfb2
Tgfbr1
Tgfbr2
Wnt5a
Wnt5b
J
Angiogenesis gene in Gcre;Igf1-f/f
CD31
KDR
EMCN
Flt1
Flt4
Vegfa

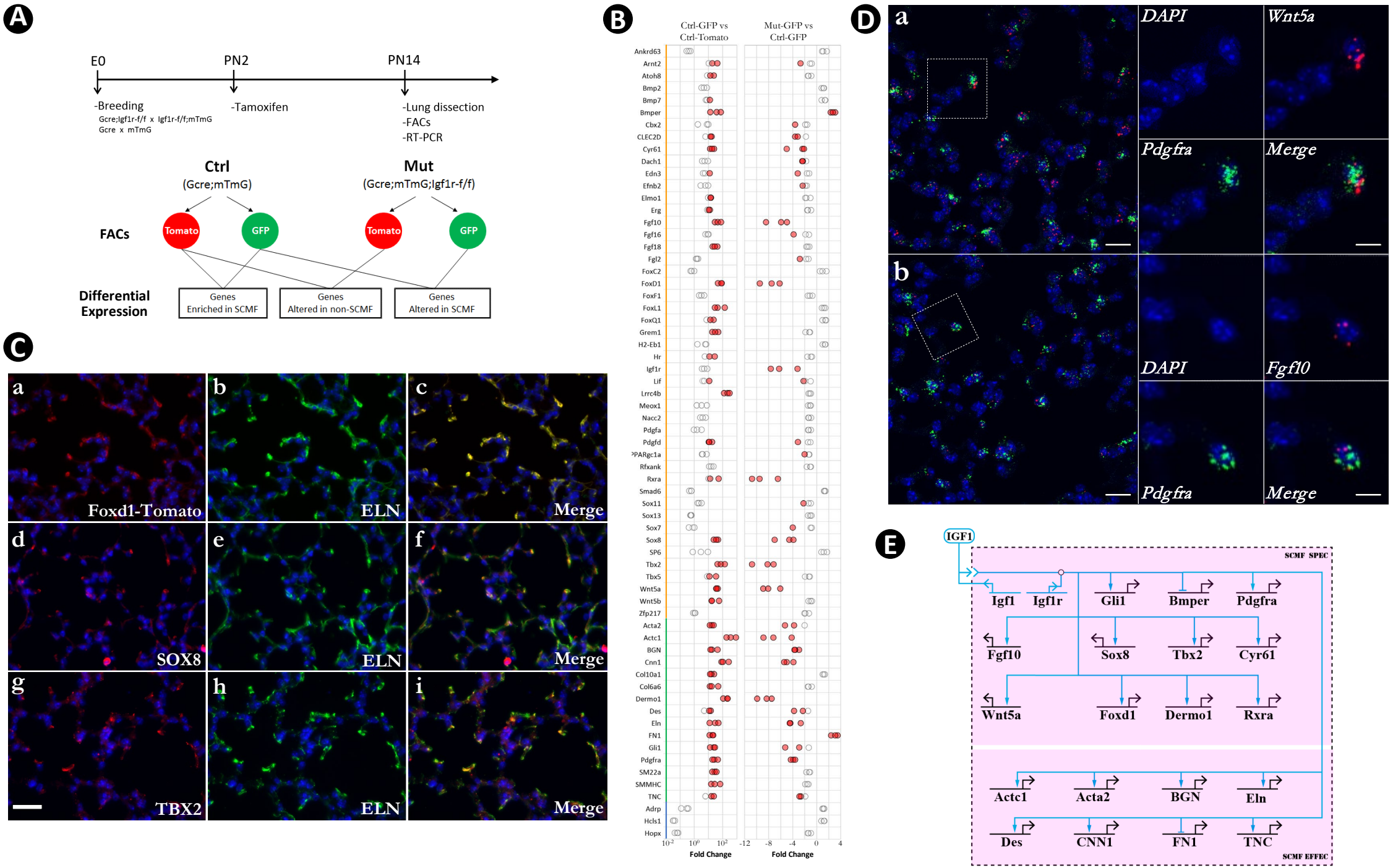
A
E0
PN2
PN14
-Breeding
Gcre;Igf1r-f/f x Igf1r-f/f;mTmG
Gcre x mTmG
-Tamoxifen
-Lung dissection
-FACs
-RT-PCR
Ctrl
(Gcre;mTmG)
Mut
(Gcre;mTmG;Igf1r-f/f)
FACs
Tomato
GFP
Tomato
GFP
Differential Expression
Genes Enriched in SCMF
Genes Altered in non-SCMF
Genes Altered in SCMF
B
Ctrl-GFP vs Ctrl-Tomato
Mut-GFP vs Ctrl-GFP
Fold Change
Fold Change
C
Foxd1-Tomato
ELN
Merge
SOX8
ELN
Merge
TBX2
ELN
Merge
D
DAPI
Wnt5a
Pdgfra
Merge
DAPI
Fgf10
Pdgfra
Merge
E
IGF1
SCMF SPEC
Igf1
Igf1r
Gli1
Bmper
Pdgfra
Fgf10
Sox8
Tbx2
Cyr61
Wnt5a
Foxd1
Dermo1
Rxra
Actc1
Acta2
BGN
Eln
Des
CNN1
FN1
TNC
SCMF EFFEC

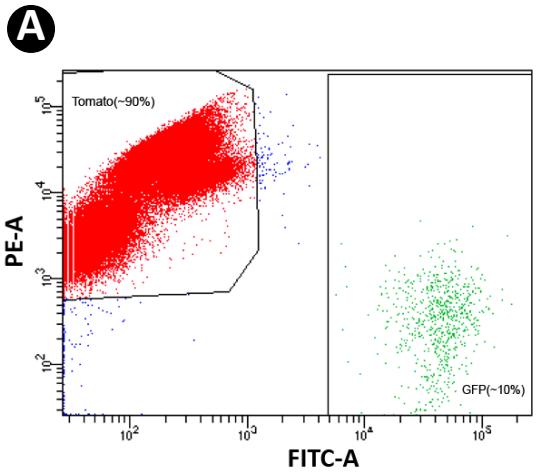
A
Tomato(~90%)
GFP(~10%)
PE-A
FITC-A

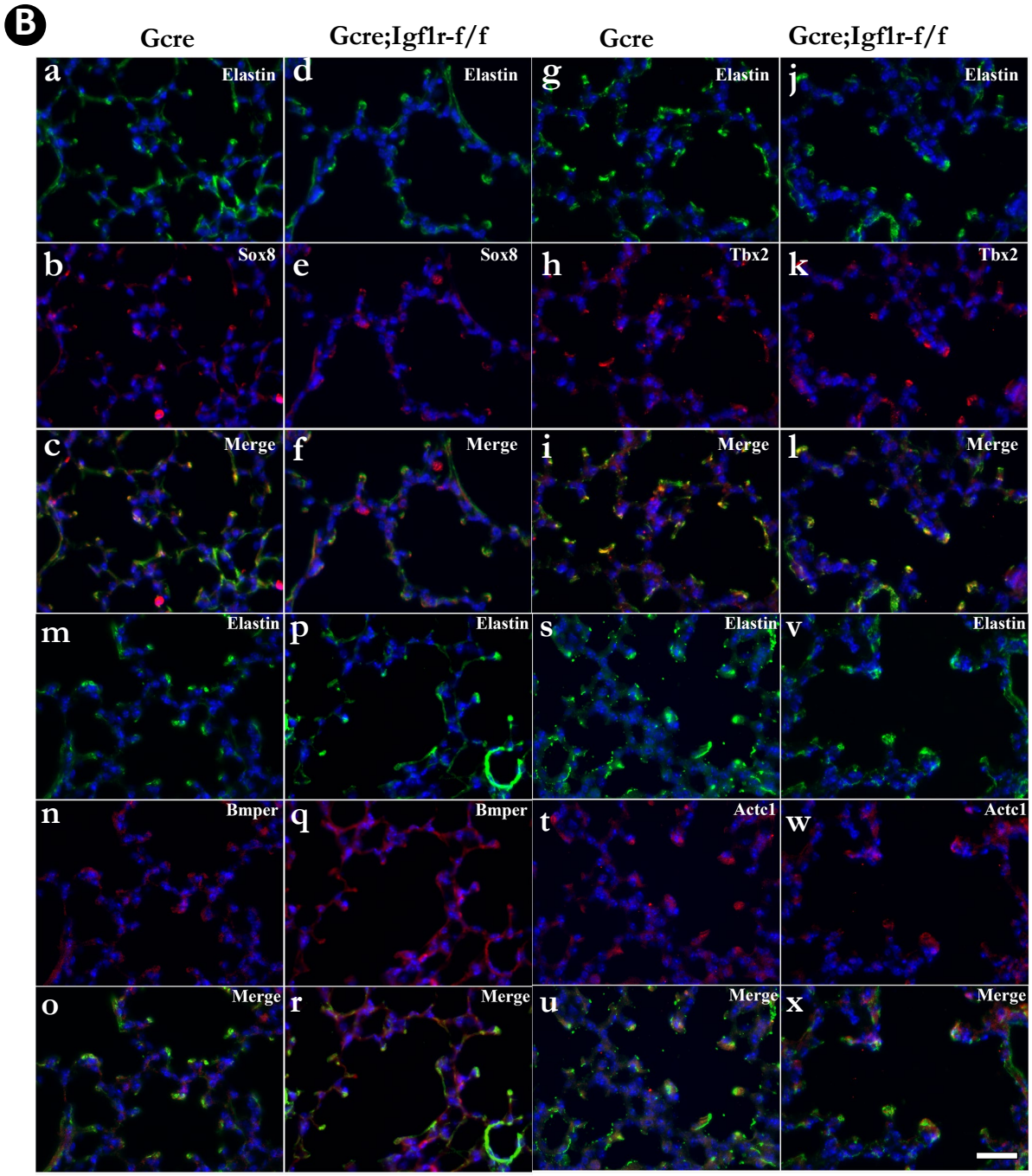
B
Gcre
Gcre;Igf1r-f/f
Gcre
Gcre;Igf1r-f/f
a Elastin
d Elastin
g Elastin
j Elastin
b Sox8
e Sox8
h Tbx2
k Tbx2
c Merge
f Merge
i Merge
l Merge
m Elastin
p Elastin
s Elastin
v Elastin
n Bmper
q Bmper
t Actc1
w Actc1
o Merge
r Merge
u Merge
x Merge

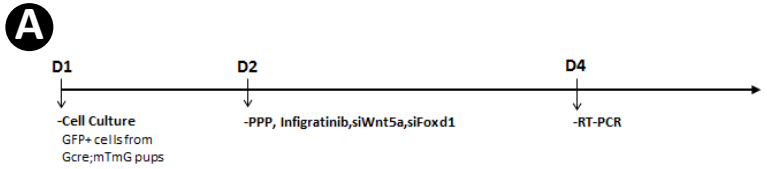
A
D1
D2
D4
-Cell Culture
GFP+ cells from
Gcre;mTmG pups
-PPP, Infigratinib,siWnt5a,siFoxd1
-RT-PCR

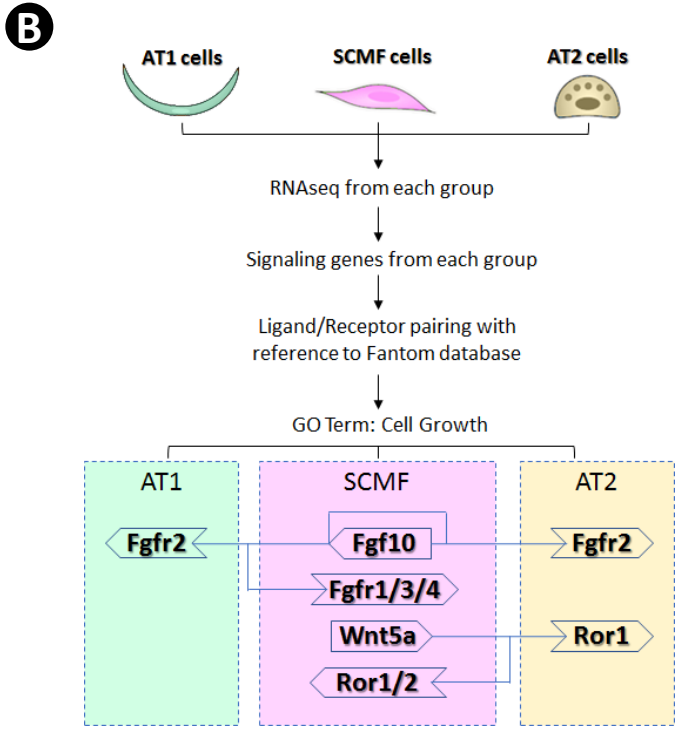
B
AT1 cells
SCMF cells
AT2 cells
RNAseq from each group
Signaling genes from each group
Ligand/Receptor pairing with
reference to Fantom database
GO Term: Cell Growth
AT1
SCMF
AT2
Fgfr2
Fgf10
Fgfr1/3/4
Wnt5a
Ror1/2
Fgfr2
Ror1

C
Infigratinib
siWnt5a
siFoxd1
Acta2
Actc1
BGN
Bmper
Cnn1
Cyr61
Dermo1
Des
Eln
Fgf10
FN1
Foxd1
Pdgfra
Rxra
Sox8
Tbx2
TNC
Wnt5a
-6
-4
-2
0
2
Fold Change

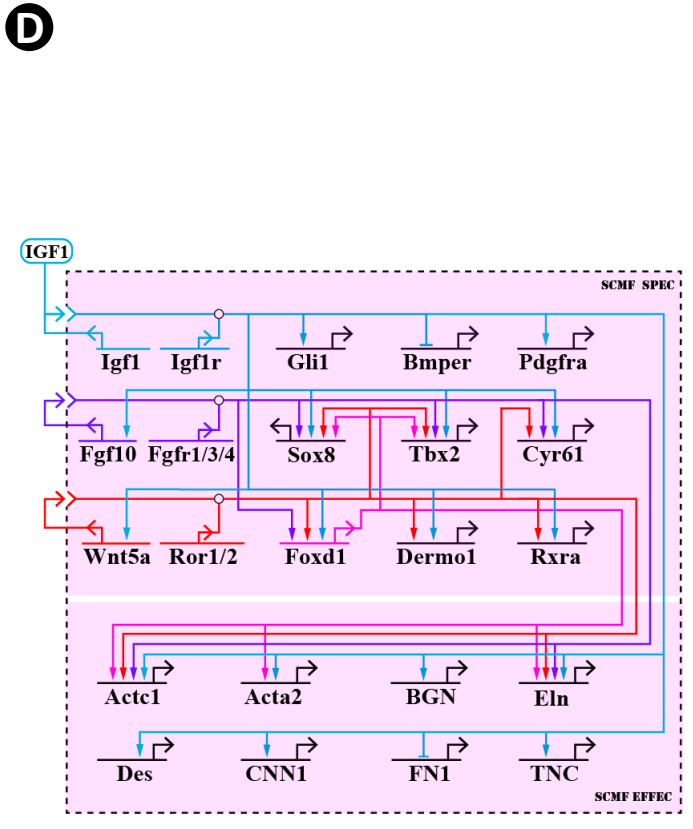
D
IGF1
SCMF SPEC
Igf1
Igf1r
Gli1
Bmper
Pdgfra
Fgf10
Fgfr1/3/4
Sox8
Tbx2
Cyr61
Wnt5a
Ror1/2
Foxd1
Dermo1
Rxra
Actc1
Acta2
BGN
Eln
Des
CNN1
FN1
TNC
SCMF EFFEC

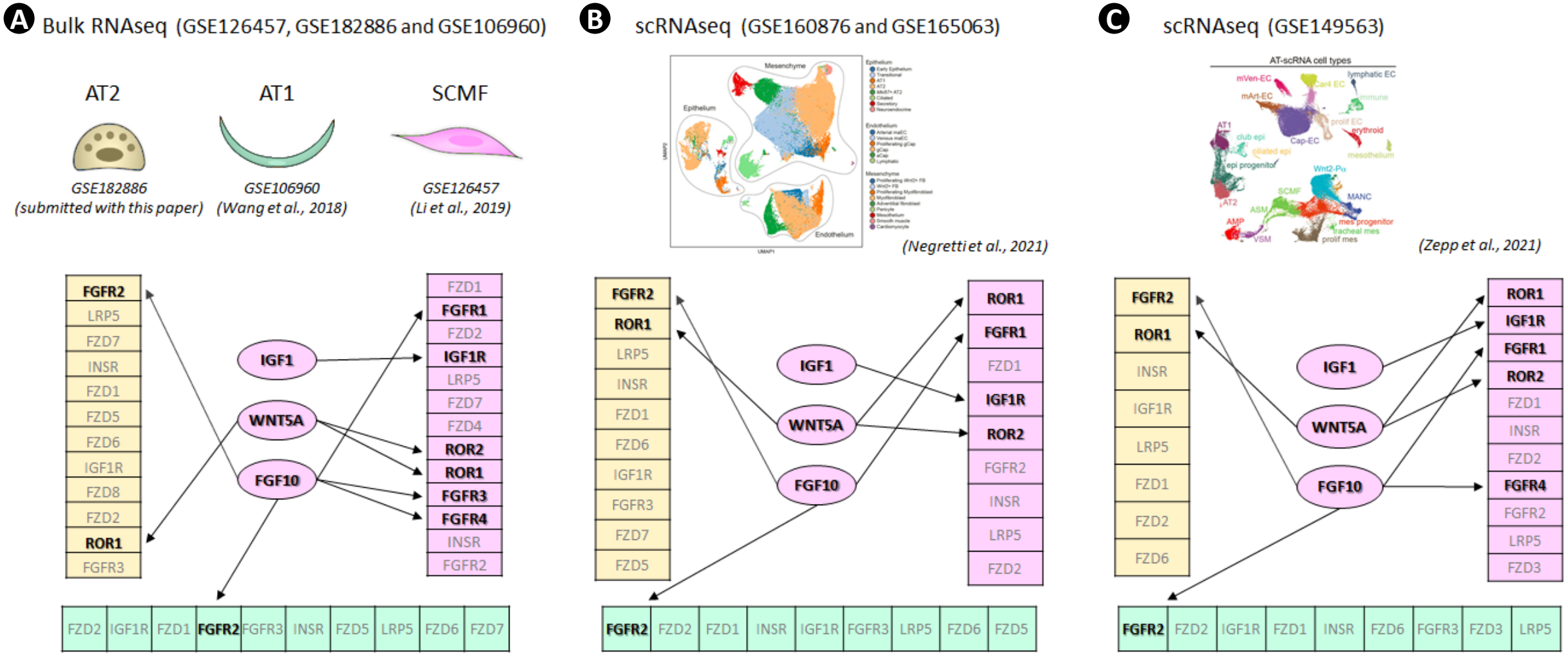
A Bulk RNAseq (GSE126457, GSE182886 and GSE106960)
AT2
AT1
SCMF
GSE182886
(submitted with this paper)
GSE106960
(Wang et al., 2018)
GSE126457
(Li et al., 2019)
FGFR2
LRP5
FZD7
INSR
FZD1
FZD5
FZD6
IGF1R
FZD8
FZD2
ROR1
FGFR3
IGF1
WNT5A
FGF10
FZD1
FGFR1
FZD2
IGF1R
LRP5
FZD7
FZD4
ROR2
ROR1
FGFR3
FGFR4
INSR
FGFR2
FZD2 IGF1R FZD1 FGFR2 FGFR3 INSR FZD5 LRP5 FZD6 FZD7
B scRNAseq (GSE160876 and GSE165063)
Mesenchyme
Epithelium
Endothelium
(Negretti et al., 2021)
FGFR2
ROR1
LRP5
INSR
FZD1
FZD6
IGF1R
FGFR3
FZD7
FZD5
IGF1
WNT5A
FGF10
ROR1
FGFR1
FZD1
IGF1R
ROR2
FGFR2
INSR
LRP5
FZD2
FGFR2 FZD2 FZD1 INSR IGF1R FGFR3 LRP5 FZD6 FZD5
C scRNAseq (GSE149563)
AT-scRNA cell types
(Zepp et al., 2021)
FGFR2
ROR1
INSR
IGF1R
LRP5
FZD1
FZD2
FZD6
IGF1
WNT5A
FGF10
ROR1
IGF1R
FGFR1
ROR2
FZD1
INSR
FZD2
FGFR4
FGFR2
LRP5
FZD3
FGFR2 FZD2 IGF1R FZD1 INSR FZD6 FGFR3 FZD3 LRP5

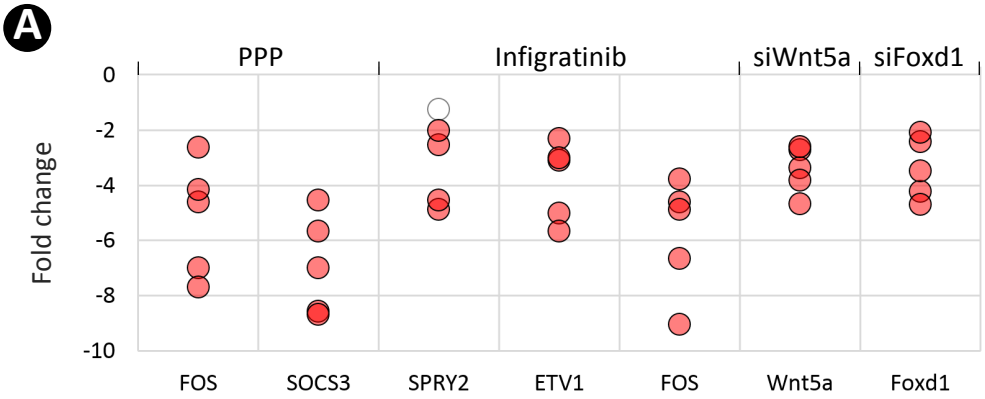
A
PPP
Infigratinib
siWnt5a
siFoxd1
Fold change
0
-2
-4
-6
-8
-10
FOS
SOCS3
SPRY2
ETV1
FOS
Wnt5a
Foxd1

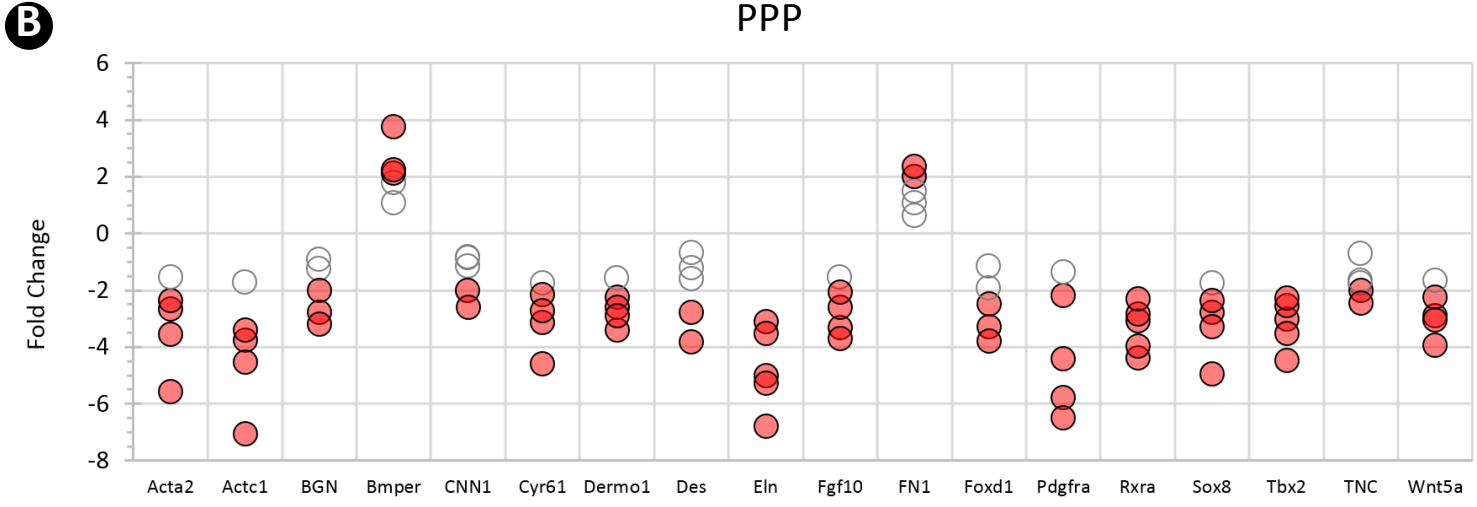
B
PPP
Fold Change
6
4
2
0
-2
-4
-6
-8
Acta2
Actc1
BGN
Bmper
CNN1
Cyr61
Dermo1
Des
Eln
Fgf10
FN1
Foxd1
Pdgfra
Rxra
Sox8
Tbx2
TNC
Wnt5a

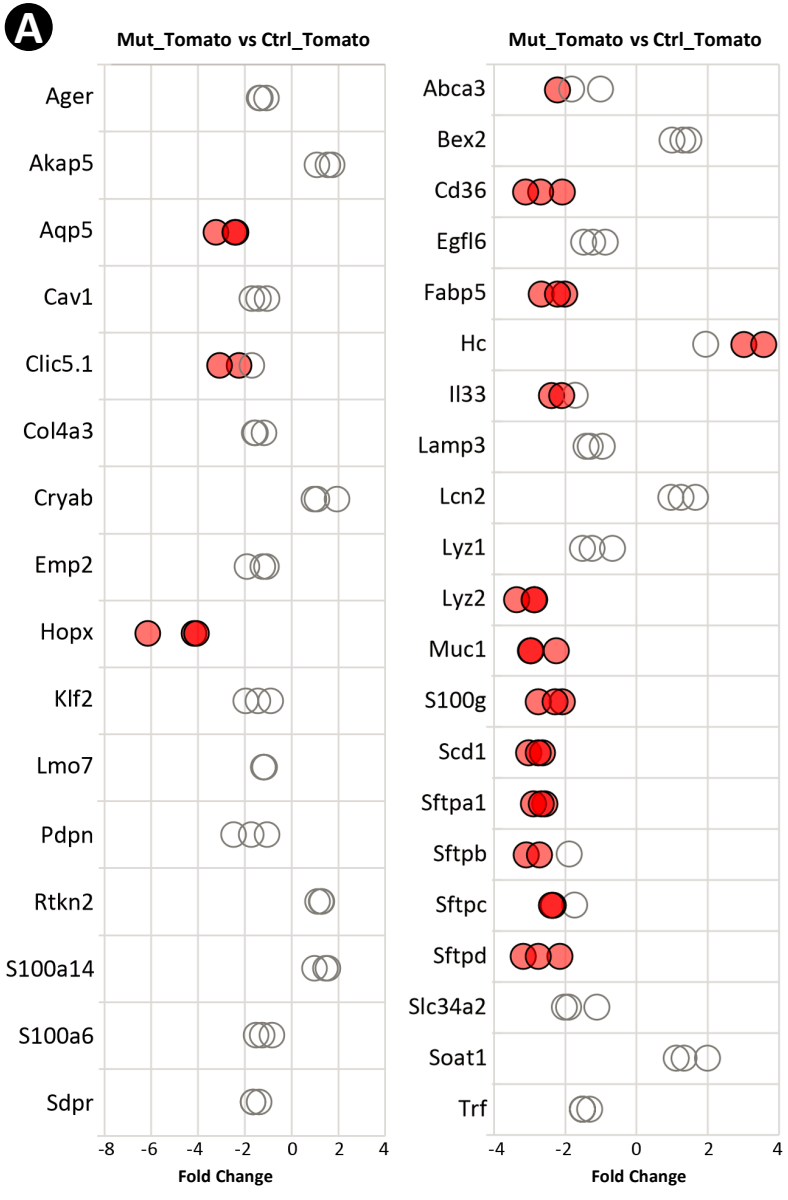
A
Mut_Tomato vs Ctrl_Tomato
Ager
Akap5
Aqp5
Cav1
Clic5.1
Col4a3
Cryab
Emp2
Hopx
Klf2
Lmo7
Pdpn
Rtkn2
S100a14
S100a6
Sdpr
-8 -6 -4 -2 0 2 4
Fold Change
Mut_Tomato vs Ctrl_Tomato
Abca3
Bex2
Cd36
Egfl6
Fabp5
Hc
Il33
Lamp3
Lcn2
Lyz1
Lyz2
Muc1
S100g
Scd1
Sftpa1
Sftpb
Sftpc
Sftpd
Slc34a2
Soat1
Trf
-4 -2 0 2 4
Fold Change

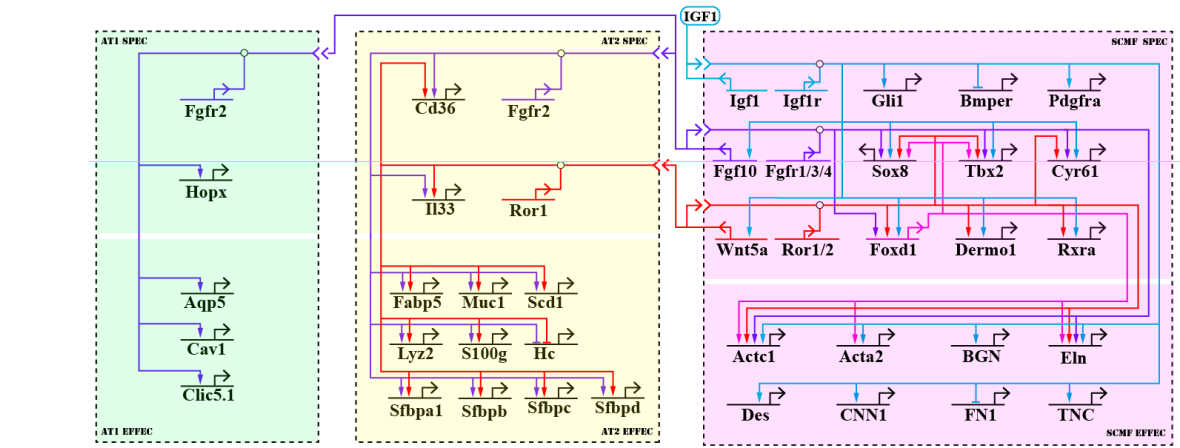
B
IGF1
AT1 SPEC
Fgfr2
Hopx
Aqp5
Cav1
Clic5.1
AT1 EFFEC
AT2 SPEC
Cd36
Fgfr2
Il33
Ror1
Fabp5
Muc1
Scd1
Lyz2
S100g
Hc
Sfbpa1
Sfbpb
Sfbpc
Sfbpd
AT2 EFFEC
SCMF SPEC
Igf1
Igf1r
Gli1
Bmper
Pdgfra
Fgf10
Fgfr1/3/4
Sox8
Tbx2
Cyr61
Wnt5a
Ror1/2
Foxd1
Dermo1
Rxra
Actc1
Acta2
BGN
Eln
Des
CNN1
FN1
TNC
SCMF EFFEC

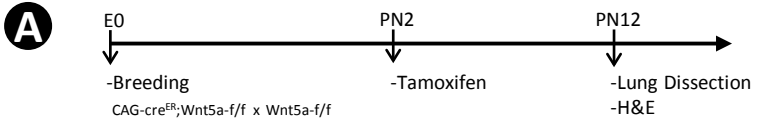
A
E0
PN2
PN12
-Breeding
CAG-cre^{ER};Wnt5a-f/f x Wnt5a-f/f
-Tamoxifen
-Lung Dissection
-H&E

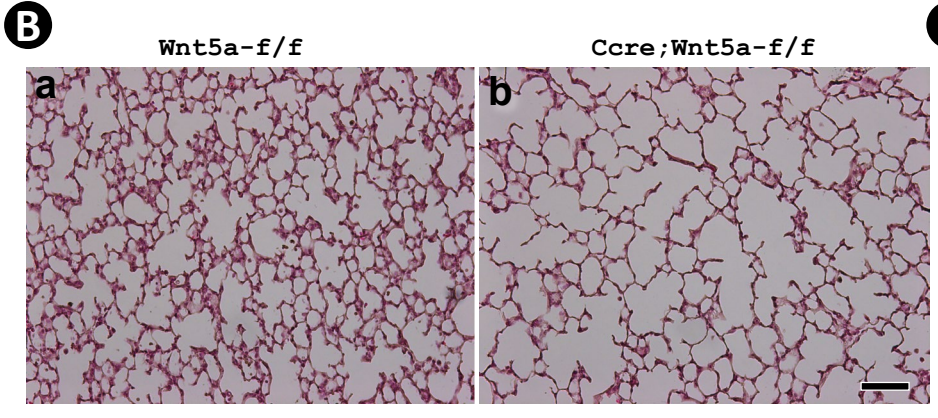
B
Wnt5a-f/f
Ccre;Wnt5a-f/f
a
b

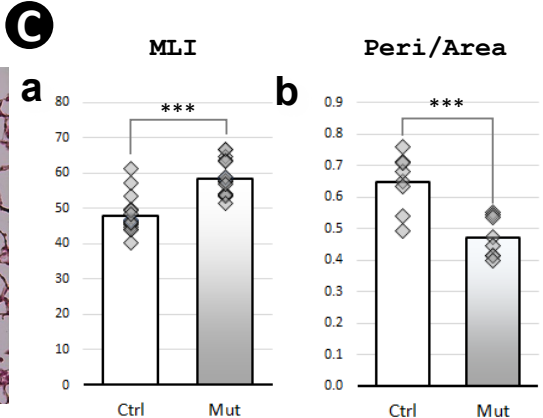
C
MLI
Peri/Area
a
b
***
***
80
70
60
50
40
30
20
10
0
0.9
0.8
0.7
0.6
0.5
0.4
0.3
0.2
0.1
0.0
Ctrl
Mut
Ctrl
Mut

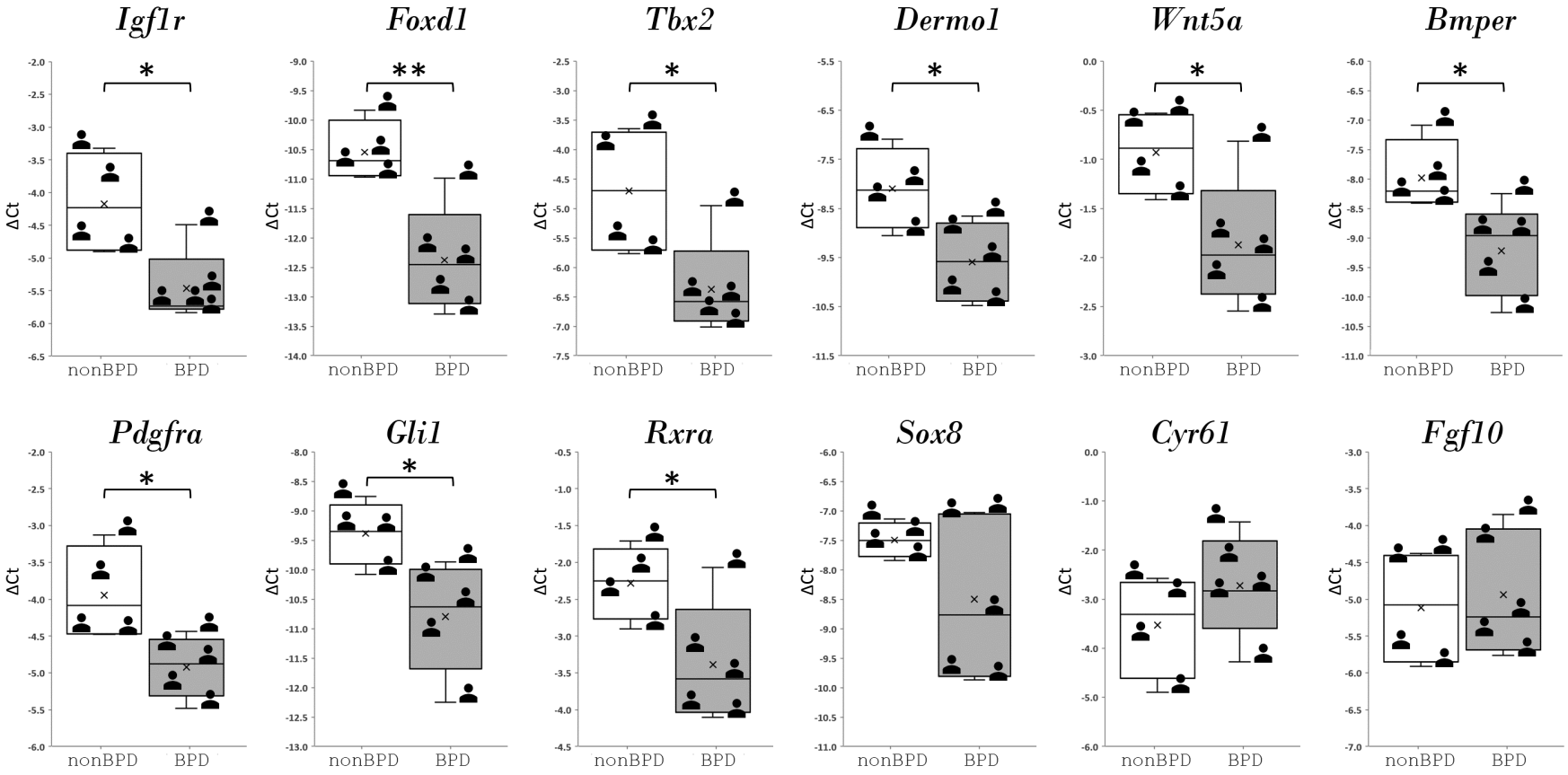
Igf1r
Foxd1
Tbx2
Dermo1
Wnt5a
Bmper
Pdgfra
Gli1
Rxra
Sox8
Cyr61
Fgf10
ΔCt
nonBPD
BPD
*
**

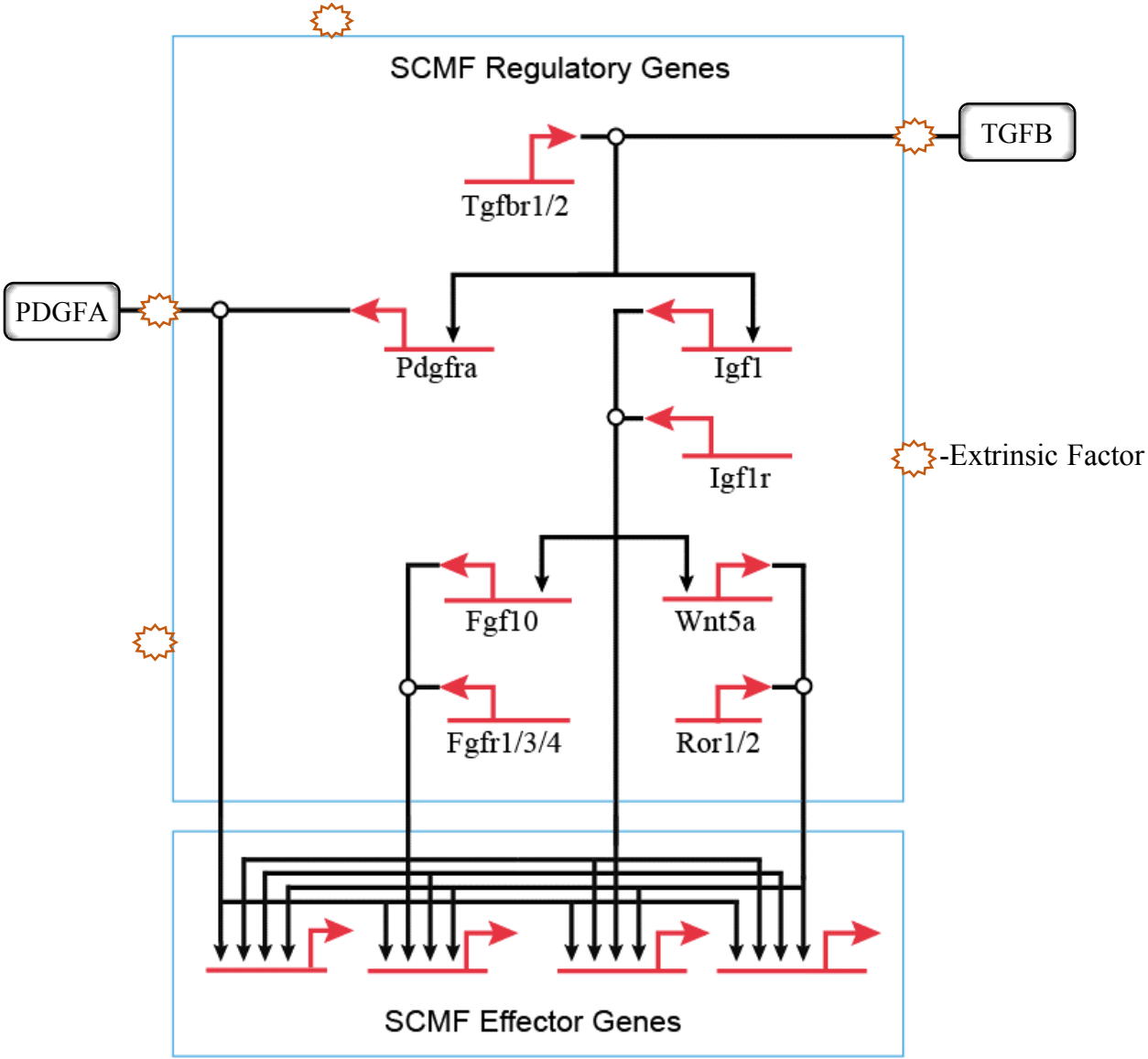
SCMF Regulatory Genes
TGFB
Tgfbr1/2
PDGFA
Pdgfra
Igf1
Igf1r
-Extrinsic Factor
Fgf10
Wnt5a
Fgfr1/3/4
Ror1/2
SCMF Effector Genes